ADVANCING EARTH AND SPACE SCIENCES

JGR Atmospheres

RESEARCH ARTICLE
10.1029/2023JD040082

Key Points:
- Introducing NASA's VIIRS Version 2 Deep Blue aerosol products
- Major updates in Deep Blue algorithm resulting in significant improvements in global aerosol optical depth retrievals
- Consistent data records between SNPP and NOAA-20+ VIIRS ensuring long-term data continuity

Supporting Information:

Supporting Information may be found in the online version of this article.

Correspondence to:

J. Lee,
jaehwa.lee@nasa.gov

Citation:

Lee, J., Hsu, N. C., Kim, W. V., Sayer, A. M., & Tsay, S.-C. (2024). VIIRS Version 2 Deep Blue aerosol products. *Journal of Geophysical Research: Atmospheres*, *129*, e2023JD040082. https://doi.org/10.1029/2023JD040082

Received 26 SEP 2023
Accepted 21 FEB 2024

VIIRS Version 2 Deep Blue Aerosol Products

Jaehwa Lee[1,2], N. Christina Hsu[2], Woogyung V. Kim[1,2], Andrew M. Sayer[2,3], and Si-Chee Tsay[2]

[1]Earth System Science Interdisciplinary Center, University of Maryland, College Park, MD, USA, [2]NASA Goddard Space Flight Center, Greenbelt, MD, USA, [3]Goddard Earth Sciences Technology and Research II, University of Maryland, Baltimore, MD, USA

Abstract NASA's Deep Blue aerosol project has developed global aerosol data records using consistent retrieval algorithms applied to various satellite sensors. The primary components of these data records are derived from the series of Visible Infrared Imaging Radiometer Suite (VIIRS) aboard the Suomi National Polar-orbiting Partnership (SNPP) and the National Oceanic and Atmospheric Administration or NOAA-20+ satellites as well as the Moderate Resolution Imaging Spectroradiometer (MODIS), among others. These instruments provide over 23 years of measurements with similar radiometric characteristics for aerosol retrievals. The algorithms used for the initial Version 1 SNPP VIIRS data set were based on the MODIS Collection 6.1 Deep Blue algorithm over land and Satellite Ocean Aerosol Retrieval (SOAR) algorithm over water. For VIIRS Version 2 data reprocessing, major updates have been made to the algorithm suite, including better accounting for effects of surface pressure, improved determination of surface reflectance, and the inclusion of fine-mode aerosol optical models to better represent anthropogenic aerosols over land. Cross-calibration gain factors are derived for the NOAA-20 VIIRS measurements to be consistent with the SNPP VIIRS, which allows the use of a unified algorithm package for both instruments. Comparisons against AERONET observations indicate that the Version 2 AOD data from SNPP VIIRS are significantly better than the Version 1 counterpart over land and slightly degraded over water in exchange for better spatial coverage. The AOD data from SNPP and NOAA-20 VIIRS are comparable, indicating that cross-calibration enables the creation of consistent aerosol data records using the series of VIIRS sensors.

Plain Language Summary Aerosols are tiny particles suspended in the air that can come from natural sources like dust and sea salt, as well as human activities such as burning fossil fuels and industrial processes. Understanding these particles are important because they play a crucial role in the Earth's system through interactions with sunlight, clouds, and precipitation. These interactions are in turn closely related to global warming and cooling effects. Additionally, certain types of aerosols can harm human health when inhaled, leading to respiratory problems. Because of these important aspects, scientists have developed various tools to study aerosols. Satellite remote sensing is one such tool and have provided valuable data on global aerosol properties. This study describes updates made to a satellite remote sensing technique to enhance data quality. The new data sets are significantly improved compared to previous versions, indicating increased utility of the data sets.

1. Introduction

Aerosols are known to play a crucial role in the Earth's climate system and air quality on multiple spatio-temporal scales (Szopa et al., 2021 and references therein). To better understand their distribution, composition, interactions with radiation, clouds, precipitation, and thus climate, numerous efforts have been made on many fronts, including retrievals of aerosol properties from space (e.g., Dubovik et al., 2019; Kaufman et al., 2002; Kokhanovsky et al., 2007; Li et al., 2009). Multispectral single-view passive sensors, for example, the Moderate Resolution Imaging Spectroradiometer (MODIS) and the Visible Infrared Imaging Radiometer Suite (VIIRS), have been widely used for their ability to make frequent global observations at a high spatial resolution of order hundreds of meters to kilometers (Cao et al., 2013; Salomonson et al., 1989). Additionally, these sensors provide relatively longer data records (together 23+ years at the time of writing), making them valuable tools for studying aerosols. The primary data that this type of sensors can provide is aerosol optical depth (AOD) at 550 nm with some skill on the particle size in terms of Ångström exponent (AE) and/or fine-mode AOD fraction (FMF).

Since its launch in 2011 aboard the Suomi National Polar-orbiting Partnership (SNPP) satellite, and later in 2017 and 2022 on the Joint Polar Satellite System or JPSS-1 and 2 satellites (renamed National Oceanic and Atmospheric Administration or NOAA-20 and 21, respectively, in final orbit), VIIRS instruments have been making measurements of the Earth with 16 spectral bands covering the visible to thermal infrared (IR) wavelength range. They have a wide swath of 3,040 km and local solar equatorial crossing time of 1:30 p.m., which allows them to observe the entire Earth twice a day (once in the daytime and once at nighttime) with overlap between consecutive swaths. VIIRS' spectral bands were carefully selected based on heritage sensors, such as MODIS, and so VIIRS can provide similar geophysical variables (including aerosols) to these heritage sensors. The current and planned series of VIIRS, in combination with MODIS (which has provided data records since December 1999 for Terra MODIS and May 2002 for Aqua MODIS), mean that long-term aerosol data records can be developed using consistent retrieval algorithms.

Several studies have used these instruments to retrieve columnar aerosol properties over land and water surfaces (e.g., Jackson et al., 2013; Levy et al., 2007, 2015; Lyapustin et al., 2018; Remer et al., 2005; Zhang et al., 2016). NASA's Deep Blue (DB) aerosol project is one such effort, which has provided a global view of aerosol properties over cloud/snow/ice-free land and water surfaces using DB-land and Satellite Ocean Aerosol Retrieval (SOAR) algorithms together. The DB/SOAR algorithm suite has successfully been applied to the Advanced Very High Resolution Radiometer (AVHRR) (Hsu et al., 2017; Sayer, Hsu, Lee, et al., 2017), the Sea-viewing Wide Field-of-view Sensor (SeaWiFS) (Hsu et al., 2004, 2006, 2013; Sayer et al., 2012), MODIS (Hsu et al., 2006, 2013), and VIIRS (Hsu et al., 2019; Lee et al., 2017; Sayer et al., 2018a) in an effort to create long-term aerosol climate data records (CDRs). Note that for MODIS, only over-land data sets are available in the current version (Collection 6.1), and discussions are underway to implement SOAR for the forthcoming Collection 7 reprocessing. Recent studies also addressed planned new aerosol products, including aerosol layer height and single-scattering albedo (SSA) using added information content from ultraviolet measurements (Lee et al., 2015, 2016, 2021) and AOD of absorbing aerosols above clouds (Sayer et al., 2016, 2019).

The initial Version 1.x (Version 1.1 being the latest; hereafter referred to as Version 1 for brevity unless stated otherwise) VIIRS DB aerosol data sets were produced using modified versions of the MODIS Collection 6.1 DB algorithm and SOAR for SeaWiFS. Major updates have since been made to the algorithms for the Version 2 data release, which are now freely available to download from NASA's Earthdata portal (https://www.earthdata.nasa.gov). These updates include better accounting for the effects of surface pressure for both over-land and over-water algorithms, and better determination of surface reflectance and new fine-mode dominated aerosol optical model together with revised SSA for the over-land algorithm.

This study provides a detailed description of the changes made to the Version 2 algorithms compared to the previous Version 1 and shows their effects on the aerosol products, mostly AOD. Section 2 summarizes updates made to the Version 2 algorithm. Section 3 provides the effects of the algorithm updates on the retrieved AOD and validation against the Aerosol Robotic Network (AERONET, Holben et al., 1998) observations. Finally, conclusions are given in Section 4.

2. Updates in the Version 2 DB/SOAR Algorithms

Comprehensive descriptions of the original VIIRS DB and SOAR algorithms are available in Hsu et al. (2019) and Sayer et al. (2018a), respectively. The algorithms are based on the principle that aerosol signals can be separated and quantified from the measured top-of-atmosphere (TOA) reflectances, which contains contributions and interactions between aerosols, surface, and other atmospheric constituents. The process uses a lookup table or LUT-based approach which retrieves aerosol properties by comparing calculated and measured TOA reflectances. The radiative transfer calculations for the LUT were performed using the Vector Linearized Discrete Ordinate Radiative Transfer (VLIDORT) code (Spurr, 2006). The general algorithm structures remain unchanged in this new version (see Figure 1 of Hsu et al. (2019) and Sayer et al. (2018a) for DB and SOAR algorithms, respectively). The algorithms work with the VIIRS moderate-resolution bands (M-bands) at a nominal spatial resolution of 750 m × 750 m at nadir and proceed through several steps to generate the Level 2 (L2, swath-level) data product, which is provided at a 6 km × 6 km resolution. The procedures include trace gas absorption correction, pixel suitability tests, surface reflectance determination, pixel-level aerosol retrieval, cell aggregation, and quality assurance (QA). The L2 data product contains 550 nm and spectral AOD, AE, aerosol type over both land and water, and additional 550 nm FMF over water. Daily and monthly Level 3 (L3) products are also produced in 1° × 1° geographic grids to facilitate applications that can benefit from lower volume, gridded data. Since aerosol properties at 550 nm are of most interest, AOD and FMF hereafter indicate those at 550 nm unless otherwise specified. In order to facilitate the discussions on changes made in the retrieval schemes, the overall structure of the DB algorithm is briefly described in order as follows.

(i) The trace gas absorption correction makes corrections to the TOA reflectances for total column water vapor and ozone as well as well-mixed gases (CO_2, CO, N_2O, NO_2, NO, CH_4, O_2, and SO_2), following the method described in Patadia et al. (2018). The Goddard Earth Observing System, Version 5 (GEOS-5) Forward Processing for Instrument Teams (FP-IT) product is used as ancillary data for determining the water vapor, ozone, and surface pressure. The data are linearly interpolated to match the VIIRS granule in space and time.

(ii) The pixel suitability test checks for pixels containing cloud/snow/ice, Sun glint, invalid observation geometry, and missing/erroneous values to find and discard pixels unsuitable for aerosol retrieval. The algorithms make retrievals only for the pixels that pass the tests (for more details see Figure 2 and corresponding text in Hsu et al., 2013 for the over-land algorithm and Section 3.2 in Sayer et al., 2018a for the over-water algorithm).

(iii) Over land, the surface reflectance is determined using one of three methods for different surface conditions determined by normalized difference vegetation index (NDVI; Tucker, 1979) and MODIS International Geosphere-Biosphere Program (IGBP) land cover type product in 0.05° grids (MCD12C1; Friedl et al., 2010):

1. The database method: Surface reflectance over bright surfaces (NDVI < 0.1) is determined using a minimum reflectance technique applied to Rayleigh- and gas absorption-corrected reflectance data aggregated in each season and 0.1° grid. This is done as a function of scattering angle and NDVI.
2. The empirical method: Surface reflectance over dark surfaces (NDVI ≥ 0.1) is determined using spectral surface reflectance relationships between the visible (490 and 670 nm) and shortwave infrared (SWIR; 2250 nm) bands as a function of NDVI.
3. The hybrid method: Surface reflectance over urban and built-up land, as determined by the MODIS IGBP land cover type, or other heterogeneous surfaces where the former two methods show limited performance is determined using the database method combined with bidirectional reflectance distribution function (BRDF) derived from atmosphere-corrected (AC) reflectance data using AERONET observations to constrain aerosols.

NDVI and $NDVI_{SWIR}$ were used to stratify the data for different vegetation conditions for the database method and the empirical method, respectively, and defined as

$$NDVI = \frac{R_{860} - R_{670}}{R_{860} + R_{670}} and \tag{1}$$

$$NDVI_{SWIR} = \frac{R_{1240} - R_{2250}}{R_{1240} + R_{2250}}, \tag{2}$$

where R is the TOA reflectance at the wavelength denoted in the subscript in nanometers. Note that the algorithm only retrieves pixels with a surface reflectance lower than the 'critical reflectance' (Fraser & Kaufman, 1985), where the sensitivity of TOA reflectance to aerosols is positive; in other words, the algorithm assumes that aerosols increase the TOA reflectance. However, the likelihood of unretrivable pixels is quite low for the 410 nm band, which emphasizes the usefulness of that band over bright surfaces.

Over water, the surface reflectance is determined by an updated water BRDF model (Sayer et al., 2018a) with near-surface wind speed (from the GEOS-5 model) and climatological chlorophyll *a* concentration as input.

(iv) The pixel-level retrieval involves the use of LUTs that contain spectral TOA reflectances as a function of various parameters affecting the TOA reflectance, that is, observation geometry, AOD at individual 410, 490, and 670 nm bands, aerosol optical model, and surface reflectance over land; observation geometry, AOD at 550 nm, FMF, aerosol optical model, wind speed, and chlorophyll *a* concentration over water.

Over land, spectral AOD is retrieved by minimizing the difference between the measured and calculated reflectance for individual bands (410, 490, and 670 nm over bright/heterogeneous surfaces or 490 and 670 nm over dark surfaces) given predefined aerosol optical model (fine-dominated or dust with varying SSA as a function of AOD in each geographic region). AE is calculated from the retrieved spectral AOD (using 410–490 nm pair over bright surfaces or 490–670 nm pair over dark surfaces) and is used to convert the spectral AOD to 550 nm AOD.

Over water, AOD, FMF, and aerosol model (marine, fine-dominated, dust, and mixed types) are simultaneously retrieved by minimizing the sum of square residuals of spectral reflectances using the Levenberg-Marquardt method (Levenberg, 1944; Marquardt, 1963). Seven VIIRS bands at 490, 555, 670, 865, 1,240, 1,610, and 2,250 nm are used over clear water (referred to as the full retrieval), and the four longer bands (865–2250 nm) over turbid water (referred to as the backup retrieval). AE is determined using precalculated spectral AOD table given retrieved AOD, FMF, and aerosol model.

(v) In the cell aggregation process, 8 × 8 retrieval "pixels" are aggregated to form retrieval "cells" at a nominal resolution of 6 km × 6 km. The mean values are reported over land, and the median over water.
(vi) The quality assurance procedure tests the number of valid retrievals, AOD variability within cells and neighboring cells, and adjacency to invalid cells. QA is assigned 1, 2, or 3 over land for poor, moderate, and good retrievals, and 1 or 3 over water for poor and good retrievals. AOD data with QA ≥ 2 are generally recommended for use for quantitative analyses and provided in separate scientific data sets called "Best Estimate". These QA filtered data sets are used in this study unless stated otherwise.

In Version 2, modifications are made to better account for the effects of surface pressure over both land and water, as well as to determine surface reflectance and aerosol optical models more accurately over land. New pixel-level AOD uncertainty estimates are added to the data product, and NOAA-20 VIIRS data set is provided in addition to that of SNPP VIIRS. Note that NASA's Earth science data collections including the Deep Blue aerosol products for SNPP and NOAA-20 VIIRS are freely available at the Earthdata portal (https://earthdata.nasa.gov).

2.1. Surface Pressure

It is important to account for variations in surface pressure (i.e., Rayleigh scattering) in the aerosol retrieval because it can make significant changes to the TOA reflectances, especially at shorter visible wavelengths. The DB and SOAR algorithms rely heavily on visible bands, making it necessary to add additional surface pressure nodes to the LUTs to better quantify the effects of changing surface pressure on the Rayleigh/aerosol interactions. In previous versions, the standard sea-level pressure (1,013.25 hPa) was assumed, meaning that the surface elevation was neglected, due to concerns about computation time and the limited maximum number of array dimensions of the Fortran language (in which the present algorithms are written). However, with increased computing power and code revision, new surface pressure nodes of 700 hPa and 900 hPa were added to the land and water LUTs, respectively, in addition to 1 atm.

The surface pressure is determined either by the GEOS-5 model over relatively flat terrain including water surfaces or the barometric formula over rugged terrain such as mountainous regions. The barometric formula is expressed as

$$p \approx p_0 \cdot \exp\left(-\frac{g \cdot h \cdot M}{T_0 \cdot R_0}\right), \tag{3}$$

where p_0: the standard sea-level pressure (1,013.25 hPa), g: gravitational acceleration (~9.81 m/s^2), h: surface elevation in meters, M: molar mass of dry air (~0.029 km/mol), T_0: standard sea-level temperature (288 K), and R_0: universal gas constant (~8.314 J/mol·K). The rugged terrain is defined as the standard deviation of surface elevations that is higher than 40 m in each 0.1° × 0.1° grid. The surface elevations are obtained from the 2-min Earth Topography data (ETOPO2; NOAA National Geophysical Data Center, 2006). This enables accounting for pressure changes due to weather patterns and mitigating errors due to the low spatial resolution (0.625° × 0.5°) of the model data. This update results in increased AOD over high elevation regions or areas under the influence of low-pressure systems (<1 atm) and vice versa.

2.2. Surface Reflectance

Surface reflectance is one of the largest error sources in retrieving AOD over land as it makes a significant contribution to the TOA reflectance. Updates were made to all three methods used in DB for determining surface reflectance (the database, empirical, and hybrid methods). First, the surface reflectance database used over bright surfaces is recreated to include the spectral surface reflectance relationships between the visible (410, 490, and 670 nm) and SWIR (2,250 nm) bands in each 0.1° grid, in addition to surface reflectance as a function of scattering angle as in the original database. This is done by searching data points with minimum Rayleigh-corrected (RC) reflectances at 490 nm ($R_{RC,\ 490}$), as a function of $R_{RC,\ 2250}$ from an extended period of time, and then applying second-order polynomial fits to the corresponding data points for each wavelength (410, 490, and 670 nm). Some examples of the spectral relationships are shown in Figure 1. The 490 nm band is used as reference because it has a stronger aerosol signal than the 670 nm band and weaker Rayleigh scattering than the 410 nm band, which reduces errors associated with the procedure. More specifically, five years of global VIIRS observations from 2013 to 2017 are filtered for clouds and corrected for Rayleigh scattering and gas absorption. The data are then averaged in 0.1° grids and sorted in each bin with a $R_{RC,\ 2250}$ width of 0.015. The second smallest $R_{RC,\ 490}$ value (shown in red diamonds in Figure 1) is selected as surface reflectance for bins that contain more than 5 data points. The select $R_{RC,\ 490}$ values are tested for outliers and passed for the polynomial fits if the number of valid data points (red diamonds) are higher than 3. The standard error of the fit ($\sigma_{\bar{x}} = \sigma/\sqrt{n}$, where σ is the standard deviation of the residuals between the measurements and the fit and n the number of data points) is also stored to test the goodness of the fit, and data with $\sigma_{\bar{x}} < 0.01$ are only used. The database created in each season is primarily used in the retrieval, with the "annual" database (from all available data regardless of season) as backup to fill in the missing values in the seasonal database and also to cover regions that require longer time series for better performance (part of Asia, North Africa, Arabian Peninsula, and Australia).

Figure 2 shows global distributions of the spectral surface reflectance relationships between the visible and SWIR bands in terms of median ratios (i.e., median ratio of the red diamonds in Figure 1). Data derived for the annual database are shown. It should be noted that the median ratios shown here are only for demonstration purposes, as it is not straightforward to show the polynomial fits. The second-order polynomial fits described above are used in the retrieval. The spatial variability of the spectral relationships illustrates the need for methodologies that can account for different surface types as well as changing surface phenology for better determination of surface reflectance, which the database method can serve. The increasing trend of the spectral ratios with wavelength indicates the advantages of the blue bands in aerosol retrieval compared to the red band. Particularly, the ratios are relatively lower over part of bright surfaces (e.g., part of North Africa, Arabian Peninsula, and Australia) than

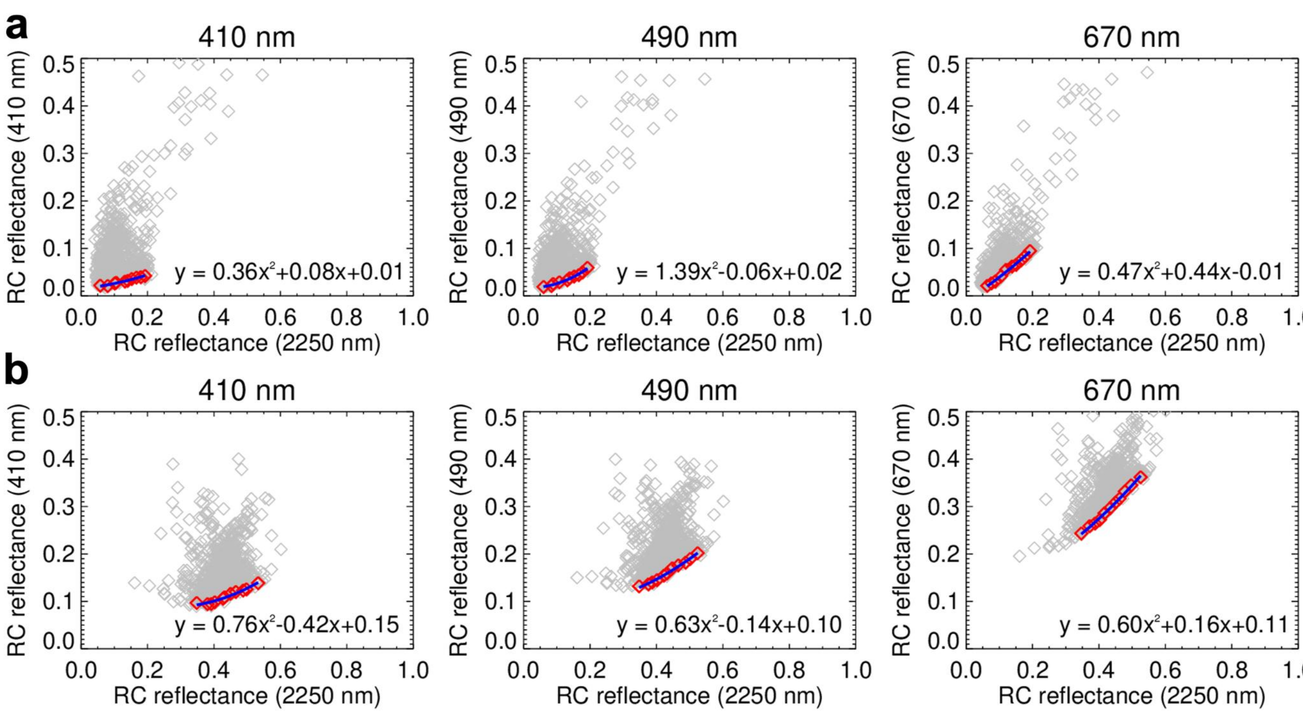

Figure 1. Spectral surface reflectance relationships between visible (410, 490, and 670 nm) and SWIR (2250 nm) bands over (a) forest in West Virginia, USA (38.35°N, 81.25°W) and (b) the Taklimakan Desert (38.85°N, 83.05°E) derived using RC reflectances from 2013 to 2017.

Journal of Geophysical Research: Atmospheres 10.1029/2023JD040082

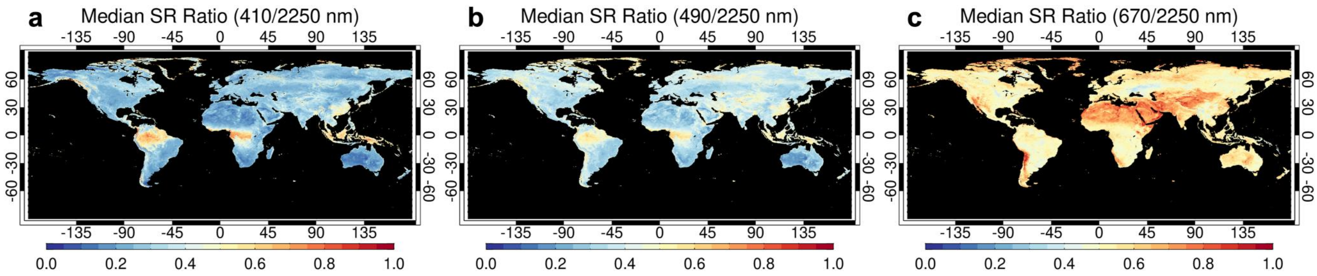

Figure 2. Median surface reflectance ratio between visible and SWIR bands for the annual surface database.

dark in the blue bands, and the opposite is true for the red band. This further emphasizes the usefulness of the blue bands, particularly over bright surfaces. Note that although the variability in the spectral ratios is mostly from real surface features, persistent cloud cover (e.g., in the tropics) and aerosol contamination (polluted regions) can increase the ratio, thereby increasing surface reflectance. This can be partly compensated for by the other two methods used in DB.

In the retrieval process, surface reflectance is derived for each retrieval pixel using the relationships with the measured $R_{RC,\ 2250}$ as the predictor. This way both the surface BRDF and changes in underlying surface conditions, for example, vegetation change, can be better described than the original approach, which partially accounted for the BRDF using the scattering angle and the vegetation change using discrete NDVI. We found that the new database has skill over vegetated surfaces as well, and thus it not only replaces the original database for the retrievals over bright surfaces ($\text{NDVI}_{\text{RC}} \leq 0.3$) but also works together with the empirical method (described below) over vegetated surfaces ($\text{NDVI}_{\text{RC}} > 0.3$). NDVI_{RC} is the same as NDVI except for using RC reflectances for mitigated angular dependence.

Second, the empirical method, similar to the one used in the Dark Target (DT) algorithm (Kaufman et al., 1997; Levy et al., 2007), has served as a simple yet useful tool to derive the surface reflectance over dark vegetated surfaces. The original algorithm worked with two sets of precalculated coefficients as a function of $\text{NDVI}_{\text{SWIR}}$. One set of which is to convert the $R_{RC,\ 2250}$ to surface reflectance at 670 nm ($R_{SR,\ 670}$) and the other $R_{SR,\ 670}$ to $R_{SR,\ 490}$. The coefficients were derived by using AC reflectance (R_{AC}) (proxy of surface reflectance) data calculated around AERONET sites (within 0.2° in latitudes/longitudes) using the AERONET-observed AOD for constraining AOD. The median values of $R_{AC,670}/R_{RC,2250}$ and $R_{AC,490}/R_{AC,670}$ for every 0.05 NDVI_{RC} interval were stored. Data with the AERONET-observed AOD (550 nm) < 0.2 and AE (440–870 nm) > 1.0 were only used for this analysis, so that only Rayleigh correction was applied to the 2250 nm band without causing significant errors for not correcting for aerosol signals. This was necessary because AERONET lacks the SWIR channel. A limitation of this approach is that the relationships can depend on underlying surface properties particularly for low NDVI regime (sparse vegetation). Note that NDVI_{RC} is used for the data stratification instead of $\text{NDVI}_{\text{SWIR}}$ as in previous versions since it leads to insignificant impact on the retrieval as well as for consistent applications for sensors lacking the 1,240 nm band, such as current meteorological imagers on geostationary satellites (e.g., Bessho et al., 2016; Holmlund et al., 2021; Kim et al., 2021; Schmit et al., 2017).

In previous versions, the coefficients derived based upon data collected over North America were used globally without considering regional dependence (which could arise due to e.g. variations in soil and vegetation types). The new version improves on this by including regional dependence in the conversion coefficients and incorporating the database method for the retrievals over the vegetated surfaces. Specifically, the coefficients are now derived separately over North America, South America, Europe, Africa, and Northeast Asia considering the regional variability in the relationships and data availability of AERONET. Other regions that are not specified use the values derived over North America. In addition, the algorithm reports the averaged AOD from the empirical method and the database method over the vegetated surfaces to take advantage of each method, that is, less potential aerosol contamination of the empirical method and less susceptibility to varying underlying surface conditions of the database method.

Lastly, the principle of the hybrid approach remains the same in Version 2 in that it utilizes the surface reflectance from the original database at a fixed scattering angle of 135° together with surface BRDF derived using the AC reflectance (i.e., surface reflectance) data set generated around AERONET sites, which is also used for the

Table 1
Bimodal Aerosol Optical Models Used in Version 2 DB Algorithm

Aerosol type	Size distribution parameters ($r_{v,1}$, $\sigma_{v,1}$; $r_{v,2}$, $\sigma_{v,2}$)	FMF	SSA node points	Particle shape
Anthropogenic aerosols	0.17, 0.44; 2.75, 0.65 μm	0.90	0.89, 0.91, 0.94, 0.96, 0.995	Sphere
Mineral dust	0.19, 0.44; 1.70, 0.51 μm	0.15	0.89, 0.91, 0.94, 0.96, 0.995	Spheroid

Note. The real part of the refractive index of 1.5 is used for both aerosol optical models with varying imaginary part for changing SSA.

empirical method above. Both the surface database and AC reflectance data set were however recalculated using consistent LUTs with the ones used for the aerosol retrievals (consistent radiative transfer model, calculation nodes, etc.). This leads to fairly small changes in surface reflectance compared to the original.

Note that the use of a minimum reflectance technique for the database method means that it can be affected by remaining aerosol signals, particulary over regions with frequent high aerosol loading and/or cloud cover. This impact decreases with increasing surface reflectance, as the sensitivity of TOA reflectance to aerosols decreases. The algorithm switches to the empirical method over dark surfaces or the hybrid method where the other two methods show limitations. As a result, no significant impact of the remaining aerosol signals was found. Nevertheless, investigations are underway for further improvements in later versions.

2.3. Aerosol Optical Model and SSA Adjustments

The Version 1 VIIRS DB algorithm (Hsu et al., 2019) assumes one fine-mode spherical (anthropogenic aerosols) and one coarse-mode dominated nonspherical (mineral dust) optical models with varying SSA in the retrieval process. Aerosol type is predefined in each region except for heavy dust cases, for which the dust model is used. For each aerosol type, SSA is also predefined for different AOD regimes. The SSA was determined based on AOD validation results against AERONET and is within a reasonable range compared with regional analyses of AERONET inversion data (e.g., Dubovik et al., 2002). It generally decreases with increasing AOD as absorbing aerosols, such as biomass burning smoke and mineral dust, tend to increase AOD.

The heavy dust is determined using an IR technique developed by Hansell et al. (2007). Since the DB algorithm was first introduced to make retrievals over deserts (Hsu et al., 2004, 2006) and the nonspherical dust optical model was newly added to the Version 1 VIIRS DB (Hsu et al., 2019; Lee et al., 2017), the spherical model used in the earlier versions of DB was optimized for better representing the phase function of mineral dust rather than anthropogenic aerosols. Now that DB has a dedicated optical model for mineral dust since the Version 1 VIIRS algorithm, the spherical model is updated to have a more realistic size distribution of anthropogenic aerosols. Based on AERONET inversions (Dubovik et al., 2006), both the anthropogenic and dust optical models comprise bimodal lognormal volume size distributions defined as

$$\frac{dV(r)}{d\ln r} = \sum_{i=1}^{2} \frac{C_{v,i}}{\sqrt{2\pi}\sigma_i} e^{-\frac{1}{2}\left(\frac{\ln r - \ln r_{v,i}}{\sigma_i}\right)^2}, \tag{4}$$

where r: particle radius, C_v: the volume concentration, r_v: the volume mode radius, and σ: the geometric standard deviation. Note that the original spherical model assumed a monomodal lognormal distribution with the mode radius (r_v) of 0.23 μm and the geometric standard deviation (σ) of 0.37 μm. Table 1 summarizes the aerosol optical models used in the Version 2 DB algorithm.

The predefined SSA were also updated to account for the effects of revised size distribution for the new spherical model since the original values were most suitable for the original model. The change in size distribution generally requires slightly more absorption (lower SSA) for consistent results because smaller particle size means stronger backscattering than the counterpart. Since the updates regarding surface pressure and surface reflectance can also change the retrieved AOD, we thoroughly examined the AOD validation against AERONET and made necessary changes to SSA. The changes in SSA are generally within 0.01 compared to the Version 1 algorithm, and the resulting values are in line with previous studies (e.g., Dubovik et al., 2002), indicating that the new spherical model well represents the real world. Note the aerosol optical models for

SOAR remain the same, that is, marine, fine-dominated, mineral dust, and mixed types with varying FMF (Sayer et al., 2018a).

2.4. Pixel-Level AOD Uncertainty Estimates

The Version 2 products include pixel-level uncertainty estimates on the retrieved AOD. These follow the methods used in our previous works (Sayer et al., 2013, 2018b for uncertainty estimates over land and ocean, respectively) and are intended to provide a one standard deviation estimate of the uncertainty on the retrieved AOD, referred to in shorthand as the "prognostic expected error" (EE_P). In brief, quantifying the measurement and forward model uncertainty across the range of atmospheric, surface, and geometric conditions that would be needed for a full forward uncertainty propagation is difficult. As a result, estimates of the retrieval uncertainty are obtained by examining the statistics of observed retrieval errors via comparison with AERONET data across a range of conditions. This uses the same set of VIIRS-AERONET matchups discussed later in this study. The main assumption is that the AERONET matchups provide a sufficiently generalizable set that a parametrization for uncertainty can be obtained from the observed retrieval errors.

Analysis of MODIS DB data revealed that the primary factors influencing retrieval quality over land were the magnitude of the AOD, the solar/view geometry, the surface type, and the QA flag associated with the retrieval (Sayer et al., 2013). Geometry is represented as the air mass factor (AMF), $1/\mu_0+1/\mu$ (where μ_0 and μ are the cosines of the solar and viewing zenith angles, respectively), essentially the atmospheric path length. The first two of these are continuous quantities (and error tended to increase with increasing AOD and decrease with increasing AMF) while the latter two are categorical. Following Sayer et al. (2013), the prognostic expected error is then defined:

$$EE_p = \frac{a + b\tau_V}{\frac{1}{\mu_0} + \frac{1}{\mu}}, \quad (5)$$

where τ_V is VIIRS AOD. One set of coefficients a, b are determined for each sensor and each combination of the QA flag (1, 2, or 3) and surface type as surface reflectance method used (i.e., the database, empirical, and hybrid method generally representing arid, vegetated, and inhomogeneous surfaces, respectively). These coefficients are determined by first binning the data as a function of satellite-retrieved AOD and calculating the product of observed absolute retrieval error and AMF for each matchup (basically a rearrangement of Equation 5). Then, a and b are obtained fitting the 68th percentile (one standard deviation point) of these scaled absolute errors. The reason for binning is statistical: that the uncertainty is a measure of the dispersion around the retrieval, while the error is what is actually observed for a given matchup (a draw from the uncertainty distribution). Due to time series length differences, the SNPP analysis used 500 matchups per bin while the NOAA-20 analysis used 200 per bin. Resulting coefficients for the two VIIRS sensors are given in Table 2.

Over water, the approach used in VIIRS Version 1 (Sayer et al., 2018b) is followed as presented there. This is as Equation 5 except without AMF dependence, as this was found to have little predictive power, so EE_P becomes a linear function of retrieved AOD. One set of coefficients are determined for each aerosol optical model for each of the full and backup retrieval algorithms. Note that the main reason for assignment of QA = 1 over water is suspicion of cloud or land contamination, which are both non-Gaussian uncertainty sources; for that reason, the analysis is only done for QA = 3 retrievals, and the estimated uncertainties calculated by the method are doubled for QA = 1 retrievals. Coefficients for both VIIRS sensors are given in Table 3. Note that in some cases the fit intercept is small and negative, although even for an AOD of 0.01 the resulting EE_P remains positive. Furthermore, the coefficients are expected to have limited representation for extremely low or high AOD, as they were statistically derived using real-world data.

2.5. Cross-Calibration Between NOAA-20 and SNPP VIIRS Over Land

To ensure consistent aerosol data records between SNPP and NOAA-20 VIIRS (and MODIS), additional calibration adjustments are applied to the Level 1B data before the aerosol retrieval is performed. Unlike MODIS, VIIRS has a dual-gain design. Therefore, the radiometric sensitivity and corresponding calibration of the VIIRS sensor could behave differently over different radiance domains. As a result, different calibration strategy is used for land and water targets. Over water, SNPP VIIRS is cross-calibrated against Aqua MODIS for inter-sensor data

Table 2
Prognostic AOD Expected Error Coefficients in $\frac{a+b\tau_V}{\frac{1}{\mu_0}+\frac{1}{\mu}}$ *for the Over-Land Retrievals*

	SNPP		NOAA-20	
Surface type	a	b	a	b
QA = 1				
Arid	0.066	1.09	0.081	1.09
Vegetated	0.091	0.83	0.095	0.93
Inhomogeneous	0.058	0.73	0.051	0.83
QA = 2				
Arid	0.034	1.14	0.021	1.26
Vegetated	0.072	0.68	0.067	0.74
Inhomogeneous	0.062	0.57	0.063	0.57
QA = 3				
Arid	0.018	1.19	0.076	0.94
Vegetated	0.094	0.66	0.084	0.71
Inhomogeneous	0.082	0.54	0.082	0.59

Table 3
Prognostic AOD Expected Error Coefficients in $a + b\tau_V$ *for the Over-Water Retrievals*

	SNPP		NOAA-20	
Aerosol model	a	b	a	b
Full retrieval				
Maritime	0.001	0.35	−0.004	0.37
Dust	0.070	0.03	0.081	0.03
Fine-dominated	0.017	0.20	0.007	0.22
Mixed	0.037	0.16	0.020	0.20
Backup retrieval				
Maritime	−0.001	0.39	−0.002	0.36
Dust	0.088	0.01	0.092	0.02
Fine-dominated	0.018	0.26	0.005	0.27
Mixed	0.037	0.24	0.020	0.27

continuity, as SNPP VIIRS calibration was significantly higher than MODIS (Sayer, Hsu, Bettenhausen, et al., 2017). In constast, the cross-calibration is not applied to NOAA-20 VIIRS, as the resulting mean AOD offset between NOAA-20 and cross-calibrated SNPP VIIRS was found to be small (refer to Section 3.2), and the original calibration resulted in slightly better validation statistics against AERONET than those of SNPP VIIRS (refer to Section 3.3).

Over land, calibration adjustments were not made to SNPP VIIRS in both Version 1 and 2 algorithms because the calibration offset was mostly compensated by using surface reflectance derived from measured reflectance data. In Version 2, however, cross-calibration between SNPP and NOAA-20 VIIRS is performed to make the algorithm applicable to both sensors, ensuring data continuity. This has important implications for saving a significant amount of effort that would otherwise be required to create various sensor-specific tables (LUTs, surface database, etc.) and make necessary changes to the algorithms.

Specifically, the over-land cross-calibration between SNPP and NOAA-20 VIIRS is performed using collocated reflectance data in the vicinity of the 'AntarticaDomeC' AERONET site (within 200 km). The Dome Concordia (Dome-C) calibration site is favorable for this application due to its relatively well-characterized surface characteristics (flat snowpack) and small contribution of atmospheric signal (clean high-altitude environment) (Six et al., 2004). Direct comparisons between the two sensors are impractical due to the half-orbit difference (for the period used in this study) between SNPP and NOAA-20 VIIRS, which results in not only a temporal difference of approximately 50 min but also a change in observation geometry at a given location. Therefore, an indirect comparison is performed using Aqua MODIS as a transfer reference. To this end, MODIS-VIIRS pixel-level collocated 'match files' generated by the Atmosphere Science Investigator-led Processing System (A-SIPS) at the University of Wisconsin-Madison in support of the VIIRS operational data processing from January 2018 to March 2020 are used (cf. Meyer al., 2020; Sayer, Hsu, Bettenhausen, et al., 2017).

Specifically, this analysis proceeds through

1. Collocating cloud-free pixels between Aqua MODIS/SNPP VIIRS and Aqua MODIS/NOAA-20 VIIRS in time (within 10 min), space (pixel-level), and observation geometry (viewing zenith angle and scattering angle within 3°).
2. Deriving scaling coefficients (SC) for both SNPP and NOAA-20 VIIRS against Aqua MODIS, that is, $SC_{SNPP} = R_{SNPP}/R_{Aqua}$ and $SC_{NOAA\text{-}20} = R_{NOAA\text{-}20}/R_{Aqua}$.
3. Calculating the calibration gain factor for NOAA-20 against SNPP VIIRS as the ratio between SC_{SNPP} and $SC_{NOAA\text{-}20}$, thus proxy of $R_{SNPP}/R_{NOAA\text{-}20}$.

The collocated pixels are aggregated and averaged on a monthly basis to derive monthly SCs for each band. Then, the monthly SCs are averaged for the entire period (January 2018–March 2020), as no significant temporal trend or seasonal differences were found. Finally, the ratio of the SCs between SNPP and NOAA-20 VIIRS ($SC_{SNPP}/SC_{NOAA\text{-}20}$) can be deemed as the cross-calibration gain factors making the NOAA-20 VIIRS calibration in line with that of SNPP. The gain factors are summarized in Table 4. It should be noted that the gain factor for the 2250 nm band was found unstable because snow/ice absorption resulted in very small reflectance values in that band, so the value derived by Meyer et al. (2020) using water cloud targets is used instead. The original value (1.008) resulted in a slight positive offset in AOD, particularly over bright surfaces. Also noted is that fixed gain factors mean that the calibration adjustment is independent of scene brightness, which may be worth investigating in future studies.

Table 4
Cross-Calibration Gain Factors to Scale NOAA-20 VIIRS Reflectances to SNPP VIIRS

	410 nm (M01)	490 nm (M03)	550 nm (M04)	670 nm (M05)	865 nm (M07)	1,240 nm (M08)	1,610 nm (M10)	2250 nm (M11)
Gain factors	1.059	1.052	1.069	1.054	1.052	1.026	1.036	1.021

2.6. Bugfix

In addition to the major updates described above, a minor bugfix worth reporting is handling the "bowtie-deletion" pixels (Wolfe et al., 2013). To reduce the pixel distortion along the across-track scan and overlap between along-track scans, also known as the "bowtie" effect, VIIRS incorporates different aggregation methods for three different across-track zones in both directions and deletion of two and four starting and ending along-track scan lines for the outer two zones, respectively (referred to as bowtie-deletion pixels). In Version 1, the bowtie-deletion pixels were accidently counted as valid pixels in the cloud screening and QA procedures, resulting in an over-screening of retrieval pixels. After fixing the bug, the spatial coverage has increased, particularly near clouds over the high-scan angle zones (>∼32°), while maintaining retrieval accuracy.

3. Results and Discussions

3.1. Impacts of Version 2 Algorithm on Retrieved AOD

The algorithm improvements described in Section 2 have significantly enhanced the performance of retrieved aerosol products on both short- and long-term temporal scale. Figure 3 demonstrates an example of daily AOD from SNPP VIIRS using the updated Version 2 algorithm compared with the Version 1 counterpart over Southern Africa on 11 August 2020. The Version 1 algorithm was known to have a negative bias over this region due to its high altitude, as described in Section 2.1. This often led to limited skill in quantifying low AOD, making the algorithm simply report the lower bound of AOD (refer to the saturated blue colors over a large area in Figure 3a). The negative bias generally increases with decreasing surface pressure (Figure 3c). As shown in Figure 3b, the Version 2 algorithm significantly improves this issue by better accounting for the effects of changing Rayleigh scattering with respect to surface elevation or pressure in both inversion process and determining surface reflectances (in addition to other changes resulting from updates in surface reflectance and aerosol optical models). As a result, Version 2 AOD not only exhibits a smoother spatial distribution, but also better consistency with AERONET AOD, which are indicated by the circles in Figures 3a and 3b. The spatial coverage is also increased in Version 2 due to more retrieval cells passing the QA procedure because of less artificial spatial variabilities within and between neighboring cells as well as the bugfix in the bowtie-deletion pixels. Over ocean, the change in AOD is much less pronounced than over land because of smaller variability of surface pressure with slightly increased spatial coverage. It should be noted that the increase in spatial coverage tends to be near clouds which statistically can lead to slightly higher AOD in Version 2 (Eck et al., 2012; Quaas et al., 2010).

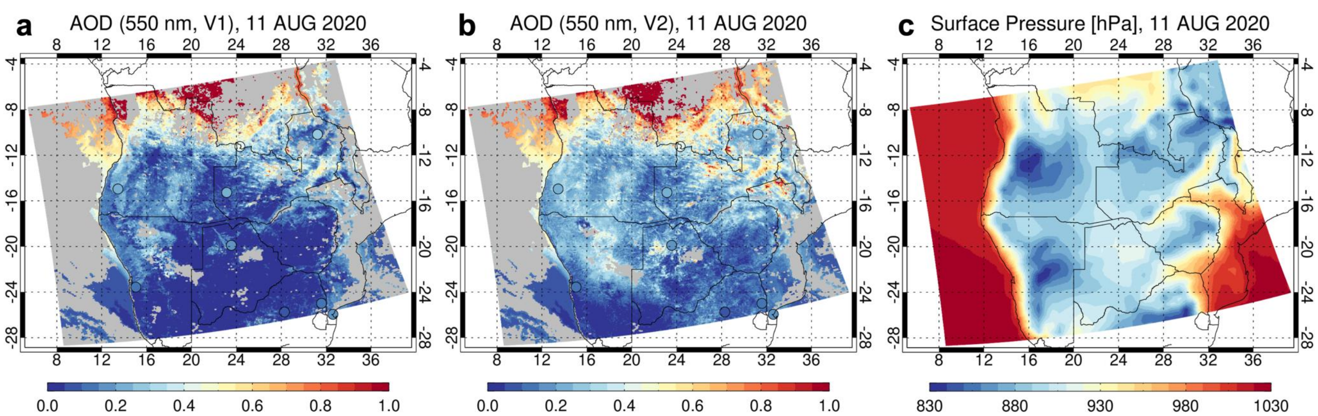

Figure 3. Examples of (a) Version 1 and (b) Version 2 AOD from SNPP VIIRS retrieved over Southern Africa, and (c) corresponding surface pressure for a 6-min VIIRS granule at 12:06 UTC on 11 August 2020. Median AERONET AOD within 30 min of the VIIRS overpass time are also shown as the circles. Invalid retrieval cells are shaded in gray.

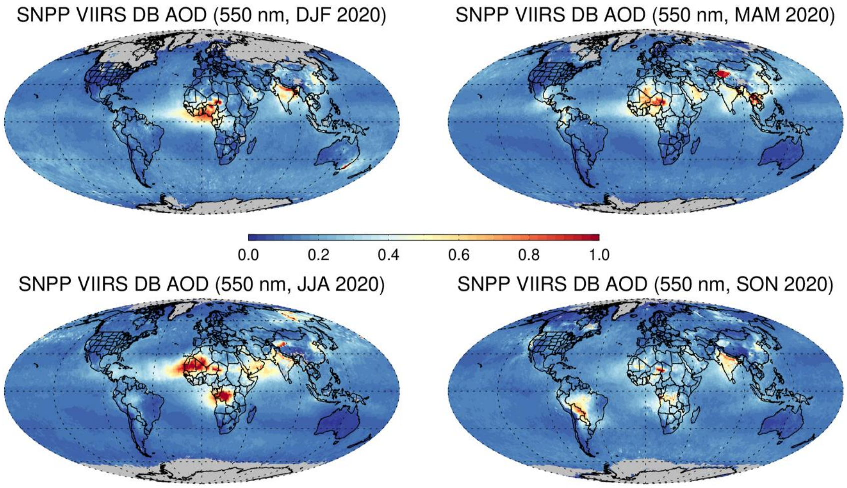

Figure 4. Global distributions of seasonal mean AOD for the SNPP VIIRS Version 2 data set in 2020. DJF: December-January-February, MAM: March-April-May, JJA: June-July-August, SON: September-October-November. Note the December data used for the DJF are from 2019.

In addition to the daily time scale, the changes in Version 2 AOD on the seasonal scale are also analyzed. Figures 4 and 5 depict the seasonal mean AOD from SNPP VIIRS in 2020 and the difference between Version 2 and Version 1, respectively. The AOD distributions (Figure 4) accurately capture the seasonal variations of major aerosol sources, such as mineral dust over North Africa and the Arabian Peninsula, biomass burning smoke over South America and Southern Africa, other anthropogenic aerosols over Asia, and marine aerosols over the Southern Ocean. The mixture of different aerosol sources often makes it difficult to distinguish between aerosol types. The long-range transport of aerosols is also adequately portrayed in the retrieved products by the smooth transitions of AOD from land to ocean. The smoothness also indicates the high fidelity of the data set over both land and water surfaces.

Figure 5 shows significant differences in Version 2 AOD compared to Version 1 over most part of the land and to a much lesser extent over ocean (generally smaller than 0.01–0.02). These changes are mostly due to the algorithm updates described in Section 2. Over land, first, the additional surface pressure node in the LUT generally increases AOD particularly over high-elevation regions, as shown in Figure 6 (e.g., western part of North and South America, Southern Africa, and Western China). This is because given AOD, the calculated TOA reflectance decreases with decreasing surface pressure; in other words, AOD needs to increase to match the observed TOA reflectance. Second, the updates in determining surface reflectances, particularly the database method,

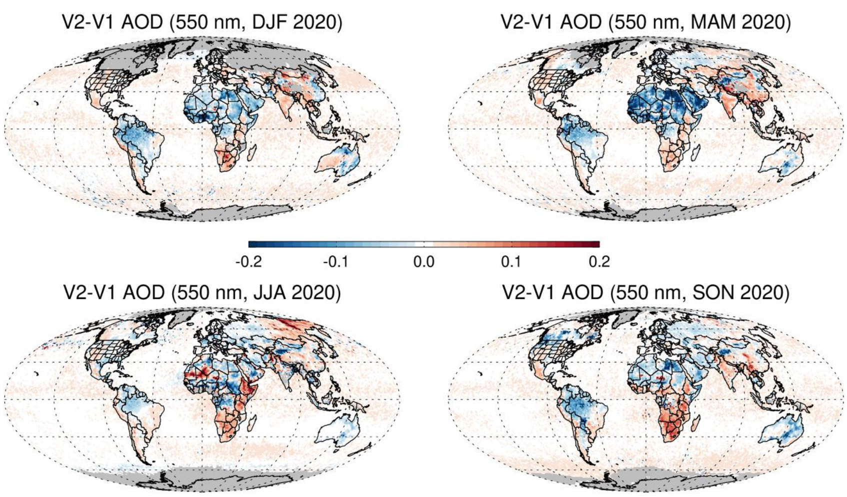

Figure 5. Same as Figure 4 except for differences between Version 2 and Version 1 SNPP VIIRS data sets.

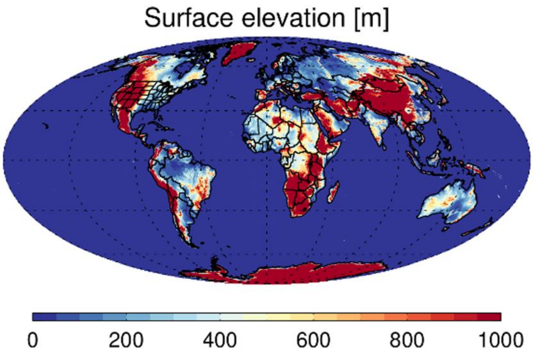

Figure 6. Global map of ETOPO2 surface elevations averaged in 0.1° grids.

generally reduce AOD over bright surfaces, such as North Africa, Arabian Peninsula, and other deserts (e.g., Taklamakan desert and deserts in Inner Mongolia and Australia). This is mainly due to increased surface reflectance by accounting for surface pressure in creating the surface database as well as finding minimum surface reflectance as a function of surface brightness ($R_{RC,2250}$) rather than only using scattering angle as in the original method. Finally, the new fine-mode dominated aerosol optical model together with SSA adjustments optimize AOD retrievals rather than creating systematic biases. The most noticeable impacts can be found over South America (smoke; decrease), India (mixed pollution; increase), and Siberia (smoke; increase). It should be noted that more than one update can have combined effects on retrieved AOD over certain regions.

The over-water algorithm only includes the update to account for the surface pressure, aside from fixing the bug in handling the bowtie-deletion pixels. As a result of this update, there are slight changes in AOD over areas with surface pressure higher or lower than the assumed 1 atm in Version 1; the higher (lower) surface pressure results in lower (higher) AOD in Version 2. Although the changes are small (mostly within 0.01–0.02), Figure 5 indicates that the increase in AOD is more prevalent and/or larger than the decrease. This is because the change in AOD is larger for lower-than-1 atm pressure (increase in AOD), and the bugfix resulted in more data coverage near clouds, for which AOD tends to be higher (Eck et al., 2012; Quaas et al., 2010).

3.2. Consistency Between SNPP and NOAA-20 VIIRS AOD

The cross-calibration ensures consistent data records between SNPP and NOAA-20 VIIRS. Our initial assessment indicated that without cross-calibration, the NOAA-20 VIIRS AOD could exhibit a significant negative offset over land when using the SNPP VIIRS-based retrieval code. This is mainly because the calibration of SNPP VIIRS is systematically higher than NOAA-20 VIIRS (Lyapustin et al., 2023; Wu et al., 2022), which results in a positive offset in surface reflectance for NOAA-20 VIIRS. Over water, the original NOAA-20 VIIRS shows comparable performance with SNPP VIIRS that is cross-calibrated against Aqua MODIS.

Figure 7 shows global distributions of seasonal mean AOD offset between NOAA-20 and SNPP VIIRS. Over land, the AOD offsets are generally small (<0.01–0.02) over areas with low aerosol loading (AOD < ∼0.2) (refer to Figure 4), indicating the successful application of cross-calibration. The offsets in both small positive and negative values (rather than showing a systematic bias) are also a good indication of the cross-calibration performing well. Over water, NOAA-20 VIIRS (which is not cross-calibrated) generally exhibit similar performance with SNPP VIIRS (which is cross-calibrated to Aqua MODIS), with a small negative offset. This is in line with

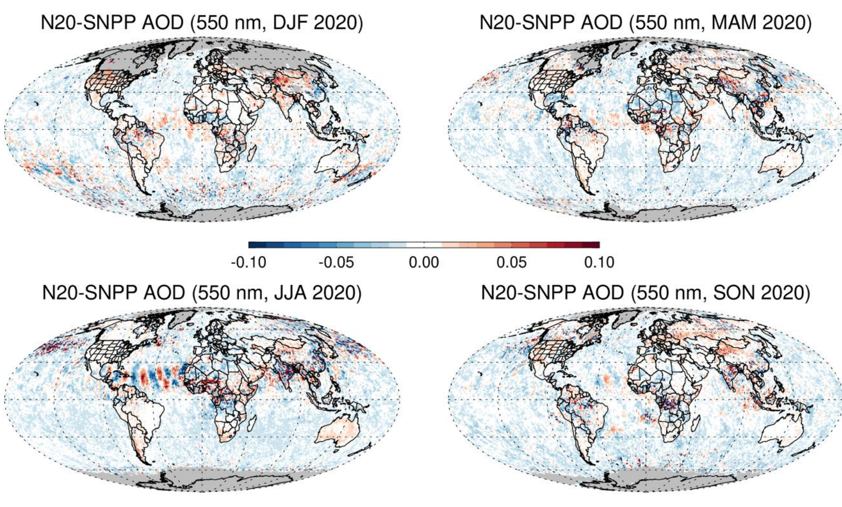

Figure 7. Same as Figure 4 except for differences between NOAA-20 and SNPP VIIRS Version 2 data sets.

the calibration characteristics of NOAA-20 VIIRS, that is, the TOA reflectances measured by NOAA-20 VIIRS are slightly darker than those of Aqua MODIS (and thus cross-calibrated SNPP VIIRS) in relevant bands (Lyapustin et al., 2023; Wu et al., 2022).

For higher AOD regime (AOD > ~0.2), assumed aerosol optical models and sampling differences between the two sensors play more significant roles and result in larger discrepancies in addition to potential increasing tendency with AOD due to residual calibration differences (note that the calibration corrections were made on a relative basis). One such example is the "wave" pattern over areas influenced by Saharan dust over the North Atlantic in JJA. Since the two sensors are in the same orbital plane with a half orbit difference (for the period presented here), the viewing swaths between them are shifted by about 1,400 km (a half of the two consecutive ground tracks), resulting in changes in data sampling and observation geometries, which, in turn, can create larger AOD differences between the sensors. The pattern is not solely from the difference in observation geometry, particularly scattering angle, since it is much less pronounced and/or shifted horizontally in other years (not shown), meaning that it can happen at different scattering angles. Overall, the median offsets range from 0.002 (JJA)–0.004 (DJF) over land, −0.007 (DJF)–−0.009 (JJA) over water, and −0.005 (DJF)–−0.008 (JJA) over both land and water, which are much smaller than inter-sensor or inter-algorithm comparisons (e.g., Sawyer et al., 2020; Sayer et al., 2018a; Sayer, Hsu, Lee, Kim, & Dutcher, 2019).

3.3. Validation Against AERONET Observations

The original Version 1 and new Version 2 VIIRS AOD data are validated against AERONET using the protocol described in Sayer, Hsu, Lee, Kim, and Dutcher (2019) to ensure consistent comparison statistics with previous studies. A brief summary is provided here. This analysis compares spatially averaged satellite AOD with temporally averaged AERONET AOD as proposed by Ichoku et al. (2002) to increase data volume, mitigate impacts of outliers, and partially account for the spatial variability of AOD. The latest AERONET Version 3 direct-Sun Level 2 (cloud-screened, post-deployment calibrated, and quality-assured) data are used (Giles et al., 2019). Using the matchups between VIIRS and AERONET data within 30 min in time, 25 km in horizontal space, and 200/100 m in altitude over land/water, the Spearman's rank correlation, median bias (MB), root mean square error (RMSE), and the fraction of matchups in agreement within the diagnostic expected error (f_{EE}) and the Global Climate Observing System (GCOS) uncertainty requirement for a climate data record (f_G) are calculated and evaluated. The diagnostic expected error (EE) is defined as ±(0.05 + 15%) over land and ±(0.03 + 10%) over water, and the GCOS uncertainty as the larger of 0.03 or 10% (GCOS, 2011). Note that the over-land diagnostic expected error (EE–note the absence of subscipted P to distinguish from the prognostic estimate provided within the files) used in this study is smaller than that for previous studies, that is, ±(0.05 + 20%) based upon the Version 1 data, since it better represents the overall uncertainty of the Version 2 data sets. Temporal periods used are from 1 March 2012–31 December 2020 for SNPP VIIRS data set, 1 January 2018–31 December 2020 for NOAA-20 VIIRS, and all available AERONET data downloaded on 28 January 2023.

The accuracy of retrieved AOD is influenced by various factors such as surface reflectance, observation geometry, and aerosol type. This leads to regional differences in the level of uncertainty of the data. The overall diagnostic EE is designed to represent the lower bound of the overall retrieval performance, and thus is heavily driven by the data over more difficult regions such as North Africa and Southeast Asia. As a result, it overestimates the typical uncertainty on a global average, that is, the algorithm does better than the EE in general. Now that the Version 2 data sets provide more sophisticated prognostic uncertainty estimates in each retrieval cell, users are encouraged to use them for quantitative applications, for example, data assimilation. The diagnostic EE together with the fraction of data within the range can still serve as a comparison metric between different satellite data sets as it is commonly used within the aerosol community (Sayer et al., 2020).

Following Sayer, Hsu, Lee, Kim, and Dutcher (2019), AERONET sites are assigned to distinct regions representing different geographic regions, surface conditions (i.e., algorithm type used and/or surface brightness), and aerosol types. Although sites with more than 50 matchups with SNPP VIIRS are shown in Figure 8, all available sites that have any matchups are used in this study unless stated otherwise (a total of 818 and 513 sites for SNPP and NOAA-20 VIIRS data sets, respectively). Note that several coastal sites have matchups for both over-land and over-water retrievals.

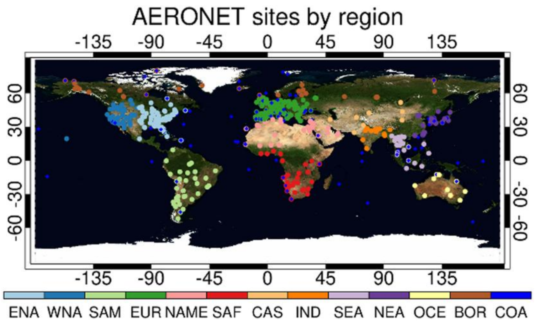

Figure 8. AERONET sites assigned for each region used in this study. Sites with more than 50 matchups between AERONET and SNPP VIIRS Version 2 data set for a period from 1 March 2012–31 December 2020 are shown. Sites shown in circles and blue diamonds are used for the over-land and over-water retrievals, respectively. ENA: Eastern North America, WNA: Western North America, SAM: South America, EUR: Europe, NAME: North America/Middle East, SAF: Southern Africa, CAS: Central Asia, IND: India, SEA: Southeast Asia, NEA: Northeast Asia, OCE: Oceania, BOR: Boreal, COA: Coastal.

3.3.1. Global and Regional Comparisons

Table 5 summarizes the global and regional evaluation metrics for SNPP VIIRS Version 1 (V1-S) and Version 2 (V2-S), and NOAA-20 VIIRS Version 2 (V2-N) AOD. Comparisons of the evaluation metrics show a significant increase in retrieval accuracy in the Version 2 data sets, except for the over-water retrievals of SNPP VIIRS, which show a slight decrease. The increase in spatial coverage, described in Section 2.6, results in larger matchups in Version 2. The NOAA-20 VIIRS data shows smaller matchups due to its shorter data record.

Over land, almost all metrics show improvement in Version 2. Globally, the RMSE of Version 2 AOD decreases by approximately 0.03, pushing the error below 0.1 (0.093 for SNPP and 0.088 for NOAA-20), with increased f_{EE} and f_G by about 0.05 and 0.06 to 0.82 and 0.54, respectively, for both sensors. The small MB of 0.004 in Version 1 decreases even further to 0.0003 for SNPP and −0.001 for NOAA-20, with increased correlation from 0.81 to 0.85 for SNPP and 0.82 for NOAA-20. Improvements are more significant in regions where the retrieval suffers more, such as North Africa/Middle East, Southern Africa, and Southeast Asia, mostly due to the updated surface database, surface pressure handling, and aerosol optical model, respectively, although the effects are combined. In Version 2, all regions except Southeast Asia over-perform the diagnostic EE of ±(0.05 + 15%), showing f_{EE} ranging from 0.66 (0.69) to 0.89 (0.87) for SNPP (NOAA-20) VIIRS, whereas Version 1 data fail to meet the EE over four regions (North Africa/Middle East, Southern Africa, India, and Southeast Asia).

Over water, the slight decrease in performance for SNPP VIIRS in Version 2 results from a slight increase in AOD due to the update to account for surface pressure and bugfix in counting the bowtie-deletion pixels. These result in marginally higher MB and RMSE (0.019 and 0.07) than those for the Version 1 (0.015 and 0.067), and lower f_{EE} (f_G) of 0.66 (0.53) compared with 0.69 (0.56) in an exchange for improved spatial coverage. In contrast, the uncertainty of NOAA-20 VIIRS over-water AOD are better than those from SNPP VIIRS,

Table 5
Comparison Statistics of 550 nm AOD Between VIIRS and AERONET Over the Regions Defined in Figure 8

	Number of matchups			Correlation			MB			RMSE			f_{EE}			f_G		
Region name	V1-S	V2-S	V2-N	V1-S	V2-S	V2-N	V1-S	V2-S	V2-N	V1-S	V2-S	V2-N	V1-S	V2-S	V2-N	V1-S	V2-S	V2-N
Global	247,894	267,830	78,525	0.81	0.85	0.82	0.004	0.0003	−0.001	0.120	0.093	0.088	0.77	0.82	0.82	0.48	0.54	0.54
ENA	37,519	39,465	12,439	0.79	0.83	0.81	0.009	−0.003	−0.003	0.080	0.064	0.062	0.83	0.88	0.87	0.55	0.64	0.62
WNA	40,732	42,378	15,625	0.55	0.70	0.64	−0.005	0.004	0.0002	0.129	0.076	0.079	0.82	0.85	0.86	0.56	0.62	0.62
SAM	14,010	15,165	2,701	0.58	0.64	0.51	−0.009	−0.002	−0.006	0.076	0.065	0.072	0.76	0.81	0.74	0.52	0.56	0.46
EUR	66,578	72,125	22,490	0.81	0.81	0.80	0.005	−0.001	−0.002	0.064	0.058	0.056	0.84	0.86	0.86	0.53	0.55	0.55
NAME	25,502	29,276	6,440	0.78	0.83	0.81	0.046	0.011	0.010	0.161	0.128	0.126	0.55	0.70	0.68	0.26	0.36	0.35
SAF	12,013	12,793	4,988	0.72	0.83	0.84	−0.026	0.005	0.004	0.129	0.101	0.107	0.62	0.76	0.73	0.35	0.45	0.43
CAS	5,660	6,158	634	0.90	0.90	0.73	−0.009	−0.007	−0.002	0.137	0.128	0.079	0.76	0.77	0.86	0.43	0.43	0.62
IND	7,164	7,631	2,114	0.90	0.91	0.90	−0.04	−0.003	−0.002	0.186	0.177	0.188	0.67	0.72	0.69	0.32	0.37	0.35
SEA	5,766	6,513	2,015	0.86	0.90	0.90	0.032	−0.001	−0.005	0.228	0.206	0.171	0.53	0.66	0.71	0.25	0.33	0.35
NEA	15,012	16,302	4,241	0.88	0.91	0.87	0.022	−0.006	−0.001	0.151	0.120	0.098	0.69	0.78	0.78	0.36	0.43	0.45
OCE	6,564	7,063	1,198	0.41	0.63	0.55	0.007	0.006	−0.005	0.087	0.050	0.059	0.74	0.86	0.84	0.51	0.64	0.56
BOR	11,374	12,953	3,639	0.82	0.79	0.77	0.007	0.0001	0.001	0.182	0.103	0.102	0.88	0.89	0.87	0.63	0.67	0.62
COA	64,545	67,506	20,460	0.87	0.87	0.86	0.015	0.019	0.011	0.067	0.07	0.065	0.69	0.66	0.86	0.56	0.53	0.58

Note. Statistics for the SNPP VIIRS Version 1 (V1-S), Version 2 (V1-S), and NOAA-20 Version 2 (V2-N) data sets are shown. Results are for the over-land retrievals except for COA for which global over-water retrievals were used.

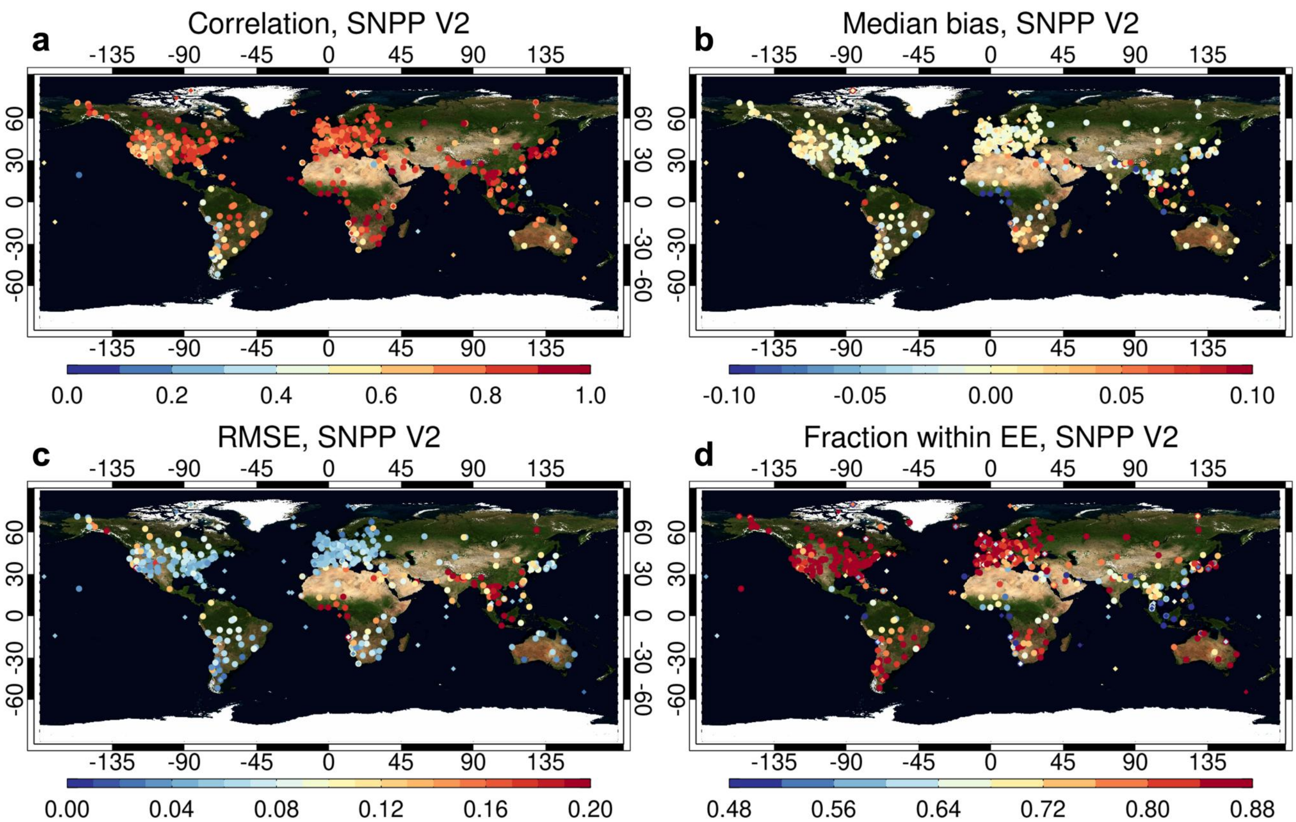

Figure 9. Comparison statistics of SNPP VIIRS Version 2 AOD at 550 nm against AERONET at individual AERONET sites. Shown are (a) the Spearman rank correlation coefficient, (b) MB, (c) RMSE, and (d) fraction of data points within the diagnostic expected error of ±(0.05 + 15%) over land and ±(0.03 + 10%) over water. Sites with more than 50 matchups are shown.

showing significantly improved metrics (MB, RMSE, f_{EE}, and f_G of 0.011, 0.065, 0.86, and 0.58, respectively) except for the correlation. The comparable correlations (0.86–0.87) between the two sensors suggest that the data sets generally have a systematic offset from each other rather than showing different variabilities in AOD, highlighting the influence of different calibrations. As calibration plays an important role in data continuity and retrieval accuracy, efforts are underway to improve the cross-calibrations between sensors as well as absolute performance (e.g., Goldberg et al., 2011; Lyapustin et al., 2023; Meyer et al., 2020; Sayer, Hsu, Bettenhausen, et al., 2017; Shea et al., 2020).

3.3.2. Comparisons at Individual AERONET Sites

Figure 9 presents the evaluation of SNPP VIIRS Version 2 data set at individual AERONET sites that have more than 50 matchups. A total of 472 and 128 sites passed the criterion for the over-land and over-water retrievals, respectively. In general, the Version 2 AOD demonstrates a high level of accuracy with small variations within each region, while inter-regional variation is much larger. This suggests that the retrieval performance is generally dependent on underlying surface conditions, aerosol properties, and observation geometries (lower latitudes tend to have lower solar zenith angle). Sites with extremely bright/inhomogeneous/rugged surfaces (lower retrieval sensitivity and/or under-constrained), high background aerosol loading/frequent cloud cover (difficult to determine surface reflectance), and/or complex aerosol types tend to underperform. The algorithm tends to struggle more over low latitude regions (Central America, North Africa, Middle East, India, and Southeast Asia) due to an additional adverse effect of lower solar zenith angle, that is, lower retrieval sensitivity. Over water, the performance is less variable and dependent more on aerosol types and turbidity of water. The evaluation metrics between the full and backup algorithms (used for clear and turbid water, respectively) are comparable (not shown), indicating that the backup algorithm works well in most cases except for some extreme cases (e.g., extreme turbidity and/or shallow water).

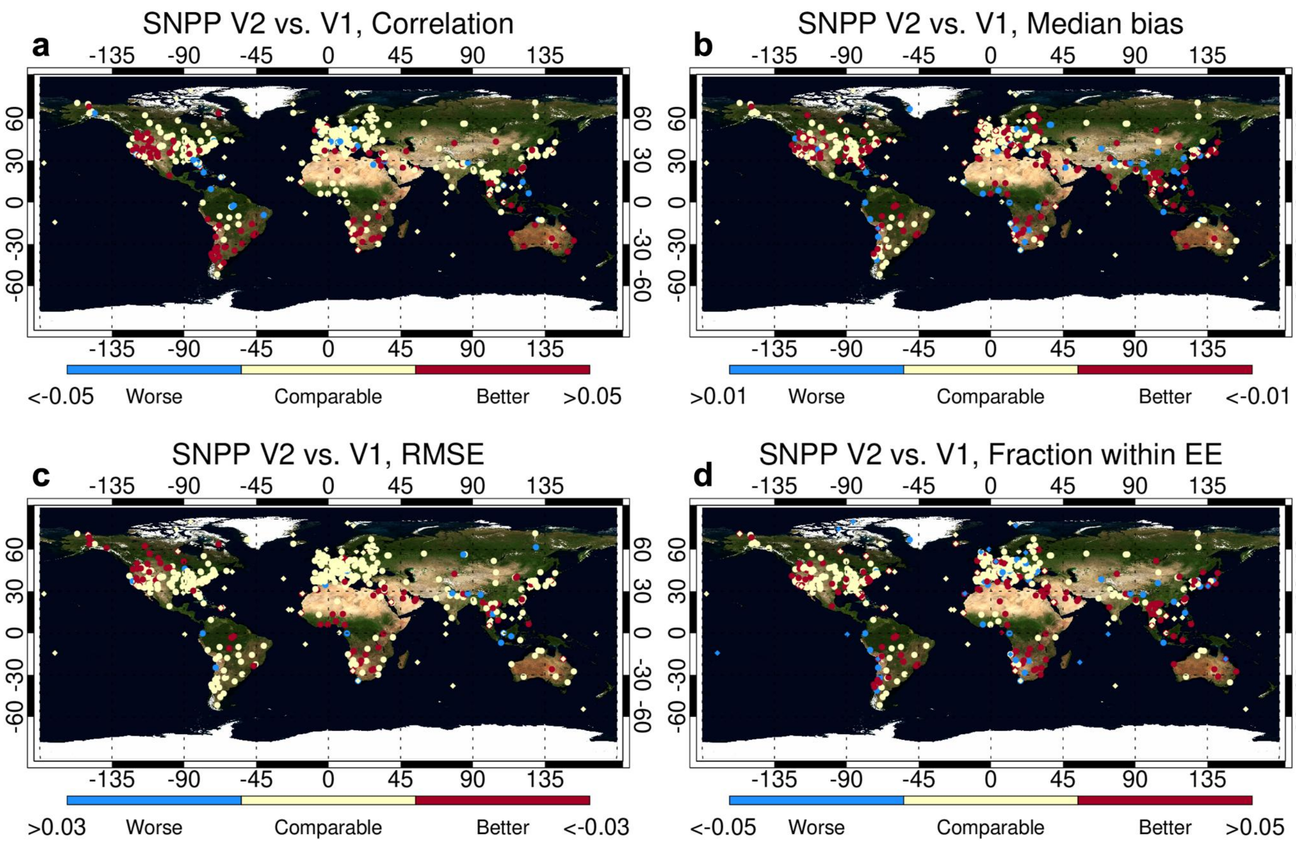

Figure 10. Performance of SNPP VIIRS Version 2 AOD compared with the Version 1 in terms of (a) correlation, (b) MB, (c) RMSE, and f_{EE}. Absolute values were used for the MB comparison. Thresholds of ±0.05, 0.01, 0.03, and 0.05 were used for the correlation, MB, RMSE, and f_{EE}, respectively.

The comparison statistics for NOAA-20 VIIRS AOD are comparable to those of SNPP VIIRS shown here and are provided in Figure S1 in Supporting Information S1. The statistics for individual AERONET sites are available to download from Lee (2024).

To further evaluate the performance gain in the Version 2 data set compared with the Version 1 counterpart, Figure 10 classifies AERONET sites into three comparative categories ('better', 'comparable', or 'worse') in terms of the evaluation metrics, and the statistics are summarized in Table 6. The differences of the evaluation metrics between the data sets (Version 2–Version 1) are tested using thresholds of ±0.05, 0.01, 0.03, and 0.05 for correlation, MB, RMSE, and f_{EE}, respectively, which are based on the differences in the global comparison statistics shown in Table 5. Then, sites are assigned to 'better', 'comparable', or 'worse' if the differences are higher, within, or lower than the thresholds. Positive values indicate improvement for correlation and f_{EE} (i.e., Version 2 values are higher), while negative values indicate improvement for MB and RMSE. Absolute values are compared for MB because it can be either positive or negative.

Table 6
Number (Fraction) of Sites for Which the Performance of Version 2 AOD Against Version 1 Falls in Each Comparative Category (Better, Comparable, and Worse) in Terms of Correlation, MB, RMSE, and f_{EE} Over Land and Water, as Shown in Figure 10

Surface type	Statistics	Better	Comparable	Worse
Land (470 sites)	Correlation	139 (0.30)	301 (0.64)	30 (0.06)
	MB	218 (0.46)	203 (0.43)	49 (0.10)
	RMSE	105 (0.22)	348 (0.74)	17 (0.04)
	f_{EE}	187 (0.40)	251 (0.53)	32 (0.07)
Water (128 sites)	Correlation	0 (0)	128 (1)	0 (0)
	MB	1 (0.01)	123 (0.96)	4 (0.03)
	RMSE	0 (0)	128 (1)	0 (0)
	f_{EE}	1 (0.01)	104 (0.81)	23 (0.18)

The Version 2 AOD performance over land is generally in line with the regional analysis mentioned earlier. A significant number of sites show improvement over bright surfaces, high elevation regions, and regions with high aerosol loadings. The number of sites with improvements is much greater than the number of sites with degradations for every metric, indicating that the improvements were achieved without sacrificing regions where the Version 1 DB performed well (e.g., Eastern North America and Europe).

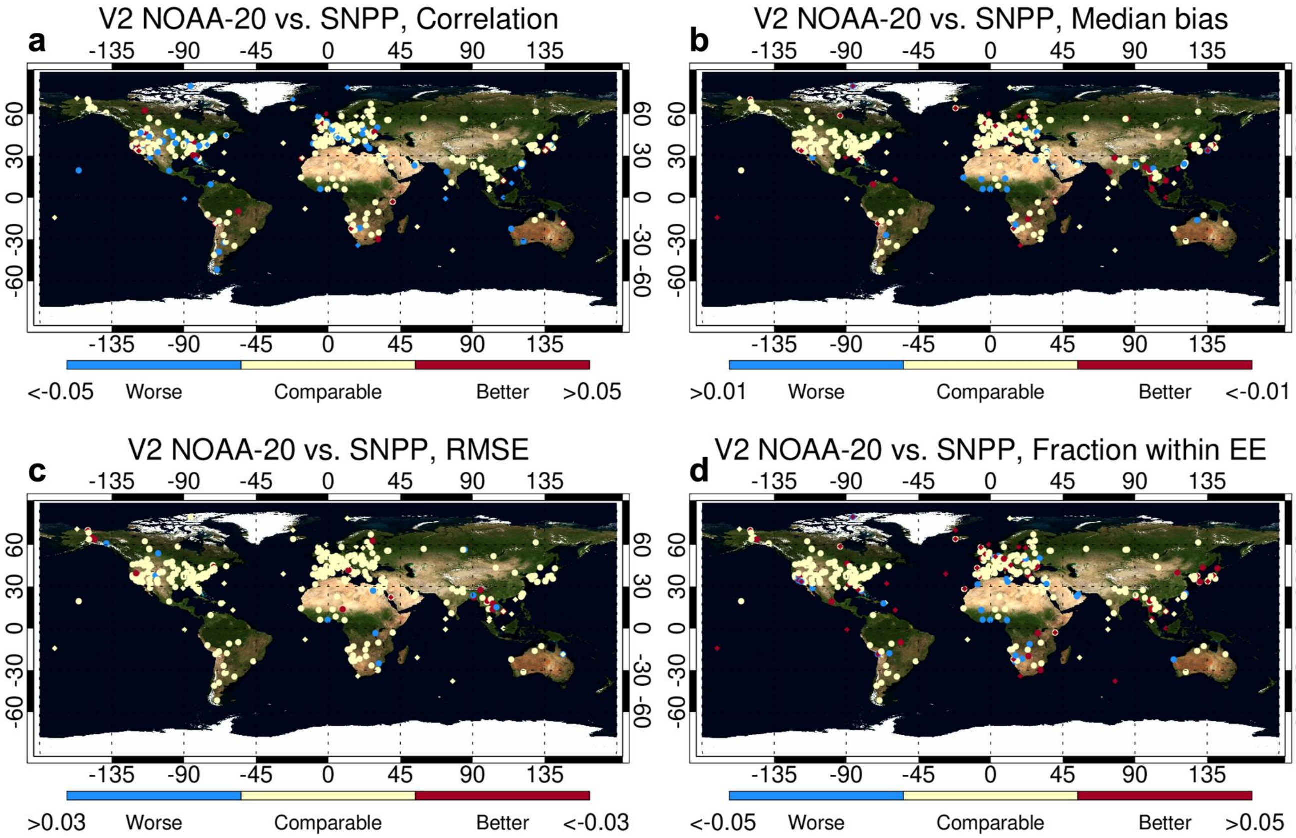

Figure 11. Same as Figure 10 except for the comparisons of the Version 2 NOAA-20 VIIRS AOD against SNPP VIIRS.

There are some degraded sites, particularly in terms of f_{EE}, which are representative of high elevation, low AOD conditions. In these cases, the Version 2 AOD shows a slight positive bias, while the Version 1 often reports a fixed lower bound AOD of 0.02 due to the systematic negative bias over high elevation regions. This is represented as better correlation and worse MB and/or f_{EE} in Version 2, for instance, over the Andes and Southern Africa. Other examples of degradation include data points near the EE bound in Version 1 which slightly move in Version 2 (comparable correlation and worse f_{EE}), an increased number of data points resulting in more scatter, small number of sites sacrificed while making general improvement, etc.

Over water, the changes in correlation, MB, and RMSE are mostly within the thresholds, indicating that the Version 2 AOD is generally consistent with the Version 1. However, the f_{EE} decreased by more than 0.05 at 18% of sites, leading the comparison metric to be classified as 'worse'. This is primarily due to the slight increase in Version 2 AOD (as shown in Figure 5 and Table 5) pusing more than 5% of data points, which were within but near the upper bound of the diagnostic expected error in Version 1, beyond the bound. This process was further exaggerated because the Version 1 AOD already exhibited a slight positive bias, meaning that there were a large number of data points near the upper bound.

The same analysis is conducted between NOAA-20 and SNPP VIIRS Version 2 AOD (NOAA-20–SNPP AOD) to reveal general consistency between the two data sets when cross-calibration is applied (Figure 11 and Table 7). Despite the different samplings in terms of observation geometry and a temporal difference of ~50 min for a fixed location resulting from the half orbit difference between the sensors, majority of sites (76%–91% depending on evaluation metrics used) show comparable performance, with similar fractions of improved (5%–9%) and degraded sites (4%–17%) over land. The comparisons (particularly MB) demonstrate some limitations of the cross-calibration particularly over bright surfaces where the adjustment amounts are larger due to higher TOA reflectance and at the same time the retrieval sensitivity is lower, such that retrieval performance can be more sensitive to remaining offsets. Since it is arguable to use SNPP VIIRS as the reference sensor, as it is known to have a positive bias, discussions are underway for better consistency.

Table 7
Same as Table 6 Except for the Performance of the Version 2 NOAA-20 VIIRS AOD Against SNPP VIIRS

Surface type	Statistics	Better	Comparable	Worse
Land (323 sites)	Correlation	20 (0.06)	247 (0.76)	56 (0.17)
	MB	15 (0.05)	284 (0.88)	24 (0.07)
	RMSE	16 (0.05)	293 (0.91)	14 (0.04)
	f_{EE}	28 (0.09)	262 (0.81)	33 (0.10)
Water (84 sites)	Correlation	6 (0.07)	59 (0.70)	19 (0.23)
	MB	41 (0.49)	40 (0.48)	3 (0.04)
	RMSE	2 (0.02)	81 (0.96)	1 (0.01)
	f_{EE}	50 (0.60)	34 (0.40)	0 (0)

Over water, NOAA-20 VIIRS AOD shows better performance, particularly in terms of MB and f_{EE}, for which 49% and 60% of sites show improvement, respectively. As mentioned earlier, this is mostly due to the difference in sensor calibration, that is, NOAA-20 VIIRS is systematically lower than the cross-calibrated SNPP VIIRS, resulting in a smaller positive bias than that of SNPP VIIRS.

4. Conclusions

The launch of the VIIRS instruments marked a new era for the Deep Blue aerosol project, which began providing aerosol data records over both land and water surfaces, unlike MODIS, which only offered over-land products. This study described major refinements made to the VIIRS DB/SOAR algorithm suite for the release of the Version 2 data set (available at https://earthdata.nasa.gov). The Version 2 data set significantly improves upon the Version 1 counterpart, particularly over land surfaces by resolving known issues in previous versions, such as systematic biases over high elevation regions and bright surfaces, and limitations in high aerosol loading cases influenced by fine-mode aerosols. This was achieved through additional surface pressure nodes in both land and water LUTs to better account for changing Rayleigh scattering, improved determination of surface reflectance, and the inclusion of fine-mode aerosol optical models with a more realistic size distribution together with further modifications of regional SSA. Cross-calibration gain factors were also derived to ensure consistent performance between SNPP and NOAA-20 VIIRS. This enabled the use of a unified algorithm package for both sensors with only minor modifications. New pixel-level prognostic uncertainty estimates were added to the data set as well.

Comparisons with AERONET observations indicate that the Version 2 AOD significantly outperforms the Version 1 counterpart over land, particularly over regions where the previous algorithm struggled more, for example, Western North America, Africa, Middle East, and Southeast Asia. The cross-calibration results in consistent performance between SNPP and NOAA-20 VIIRS data sets, with slightly larger offsets over bright surfaces and areas with high aerosol loadings. However, over water, the updates led to a slight degradation for SNPP VIIRS by worsening the positive bias in an exchange for better spatial coverage. The degradation appears to be due to sensor calibration rather than an algorithm issue, as NOAA-20 VIIRS AOD performs much better with slightly different sensor calibration. Further discussions are underway to ensure better retrieval accuracy and data continuity. It is important to note that the SNPP VIIRS was cross-calibrated to Aqua MODIS using the Collection 6.1 reflectance data, and our preliminary investigation suggests that there are nonnegligible calibration changes in the Collection 7 data, meaning that the calibration of SNPP VIIRS can change as well.

Efforts have been made to adapt the Version 2 algorithm suite to MODIS and geostationary imagers, such as the Advanced Baseline Imager (ABI) on the Geostationary Operational Environmental Satellite-R (GOES-R) series and the Advanced Himawari Imager (AHI) on the Himawari series satellites, to ensure consistent retrieval performance between sensors. This also means that the SOAR over-water retrievals are available for MODIS, and the research team is conducting extensive testing for potential inclusion of SOAR in the upcoming Collection 7 reprocessing. When achieved, the DB/SOAR aerosol products will provide a more complete picture of multi-decadal global aerosol properties spanning over the Earth Observing System (EOS) and the Joint Polar-orbiting Satellite System (JPSS) eras. Efforts are underway for future versions of VIIRS data sets, including the extension of the algorithm to NOAA-21 VIIRS, which has been operational since 30 March 2023, and retrievals of aerosol layer height and AOD above clouds and snow. In addition, new versions of AVHRR and SeaWiFS aerosol data sets are being developed to further extend the time series back to the early 1980s. These efforts will enable long-term applications of these data sets for a more comprehensive understanding of aerosol properties and their impacts on Earth system.

Data Availability Statement

The AERONET Version 3 Level 2.0 direct-Sun aerosol data used in this study are available from https://aeronet.gsfc.nasa.gov. VIIRS Level 1b, and Version 1.1 and 2 Deep Blue aerosol data are available from https://www.earthdata.nasa.gov. Note that the Version 1.1 Deep Blue data will be removed from the archive when the operation is fully moved to Version 2. The comparison statistics used in Figure 9 and Figure S1 in Supporting Information S1 are available to download from https://doi.org/10.5281/zenodo.10729462. Further information about Deep Blue is available at https://deepblue.gsfc.nasa.gov.

Acknowledgments
This research was funded by NASA's Radiation Science Program, managed by Hal Maring. The AERONET team and site Principal Investigators and managers are acknowledged for the creation and maintenance of the AERONET data record used in this study. The Atmosphere SIPS at the University of Wisconsin are thanked for VIIRS data processing.

References

Bessho, K., Date, K., Hayashi, M., Ikeda, A., Imai, T., Inoue, H., et al. (2016). An introduction to Himawari-8/9: Japan's new-generation geostationary meteorological satellites. *Journal of the Meteorological Society of Japan Series II*, *94*(2), 151–183. https://doi.org/10.2151/jmsj.2016-009

Cao, C., Xiong, J., Blonski, S., Liu, Q., Uprety, S., Shao, X., et al. (2013). Suomi NPP VIIRS sensor data record verification, validation, and long-term performance monitoring. *Journal of Geophysical Research: Atmospheres*, *118*(20), 11664–11678. https://doi.org/10.1002/2013JD020418

Dubovik, O., Holben, B., Eck, T. F., Smirnov, A., Kaufman, Y. J., King, M. D., et al. (2002). Variability of absorption and optical properties of key aerosol types observed in worldwide locations. *Journal of the Atmospheric Sciences*, *59*(3), 590–608. https://doi.org/10.1175/1520-0469(2002)059<0590:VOAAOP>2.0.CO;2

Dubovik, O., Li, Z., Mishchenko, M. I., Tanré, D., Karol, Y., Bojkov, B., et al. (2019). Polarimetric remote sensing of atmospheric aerosols: Instruments, methodologies, results, and perspectives. *Journal of Quantitative Spectroscopy and Radiative Transfer*, *224*, 474–511. https://doi.org/10.1016/j.jqsrt.2018.11.024

Dubovik, O., Sinyuk, A., Lapyonok, T., Holben, B. N., Mishchenko, M., Yang, P., et al. (2006). Application of spheroid models to account for aerosol particle nonsphericity in remote sensing of desert dust. *Journal of Geophysical Research*, *111*(D11), D11208. https://doi.org/10.1029/2005JD006619

Eck, T. F., Holben, B. N., Reid, J. S., Giles, D. M., Rivas, M. A., Singh, R. P., et al. (2012). Fog- and cloud-induced aerosol modification observed by the Aerosol Robotic Network (AERONET). *Journal of Geophysical Research*, *117*(D7), D07206. https://doi.org/10.1029/2011JD016839

Fraser, R. S., & Kaufman, Y. J. (1985). The relative importance of aerosol scattering and absorption in remote sensing. *IEEE Transactions on Geoscience and Remote Sensing, GE-*, *23*(5), 625–633. https://doi.org/10.1109/TGRS.1985.289380

Friedl, M. A., Sulla-Menashe, D., Tan, B., Schneider, A., Ramankutty, N., Sibley, A., & Huang, X. (2010). MODIS Collection 5 global land cover: Algorithm refinements and characterization of new datasets. *Remote Sensing of Environment*, *114*(1), 168–182. https://doi.org/10.1016/j.rse.2009.08.016

GCOS. (2011). Systematic observation requirements for satellite-based data products for climate, 2011 update (World Meteorological Organization (WMO) Global Climate Observing System (GCOS) report GCOS-154). Retrieved from https://library.wmo.int/doc_num.php?explnum_id=3710

Giles, D. M., Sinyuk, A., Sorokin, M. G., Schafer, J. S., Smirnov, A., Slutsker, I., et al. (2019). Advancements in the Aerosol Robotic Network (AERONET) version 3 database automated near-real-time quality control algorithm with improved cloud screening for Sun photometer aerosol optical depth (AOD) measurements. *Atmospheric Measurement Techniques*, *12*(1), 169–209. https://doi.org/10.5194/amt-12-169-2019

Goldberg, M., Ohring, G., Butler, J., Cao, C., Datla, R., Doelling, D., et al. (2011). The global space-based inter-calibration system. *Bulletin of the American Meteorological Society*, *92*(4), 467–475. https://doi.org/10.1175/2010BAMS2967.1

Hansell, R. A., Ou, S. C., Liou, K. N., Roskovensky, J. K., Tsay, S. C., Hsu, C., & Ji, Q. (2007). Simultaneous detection/separation of mineral dust and cirrus clouds using MODIS thermal infrared window data. *Geophysical Research Letters*, *34*(11), L11808. https://doi.org/10.1029/2007GL029388

Holben, B. N., Eck, T. F., Slutsker, I., Tanré, D., Buis, J. P., Setzer, A., et al. (1998). Aeronet: A federated instrument network and data archive for aerosol characterization. *Remote Sensing of Environment*, *66*, 1–16. https://doi.org/10.1016/S0034-4257(98)00031-5

Holmlund, K., Grandell, J., Schmetz, J., Stuhlmann, R., Bojkov, B., Munro, R., et al. (2021). Meteosat third generation (MTG): Continuation and innovation of observations from geostationary orbit. *Bulletin of the American Meteorological Society*, *102*(5), E990–E1015. https://doi.org/10.1175/BAMS-D-19-0304.1

Hsu, N. C., Jeong, M.-J., Bettenhausen, C., Sayer, A. M., Hansell, R., Seftor, C. S., et al. (2013). Enhanced Deep Blue aerosol retrieval algorithm: The second generation. *Journal of Geophysical Research: Atmospheres*, *118*(16), 9296–9315. https://doi.org/10.1002/jgrd.50712

Hsu, N. C., Lee, J., Sayer, A. M., Carletta, N., Chen, S.-H., Tucker, C. J., et al. (2017). Retrieving near-global aerosol loading over land and ocean from AVHRR. *Journal of Geophysical Research: Atmospheres*, *122*(18), 9968–9989. https://doi.org/10.1002/2017JD026932

Hsu, N. C., Lee, J., Sayer, A. M., Kim, W., Bettenhausen, C., & Tsay, S.-C. (2019). VIIRS Deep Blue aerosol products over land: Extending the EOS long-term aerosol data records. *Journal of Geophysical Research: Atmospheres*, *124*(7), 4026–4053. https://doi.org/10.1029/2018JD029688

Hsu, N. C., Tsay, S.-C., King, M. D., & Herman, J. R. (2004). Aerosol properties over bright-reflecting source regions. *IEEE Transactions on Geoscience and Remote Sensing*, *42*(3), 557–569. https://doi.org/10.1109/TGRS.2004.824067

Hsu, N. C., Tsay, S.-C., King, M. D., & Herman, J. R. (2006). Deep blue retrievals of Asian aerosol properties during ACE-Asia. *IEEE Transactions on Geoscience and Remote Sensing*, *44*(11), 3180–3195. https://doi.org/10.1109/TGRS.2006.879540

Ichoku, C., Chu, D. A., Mattoo, S., Kaufman, Y. J., Remer, L. A., Tanré, D., & Holben, B. N. (2002). A spatio-temporal approach for global validation and analysis of MODIS aerosol products. *Geophysical Research Letters*, *29*(12), 1616. https://doi.org/10.1029/2001GL013206

Jackson, J. M., Liu, H., Laszlo, I., Kondragunta, S., Remer, L. A., Huang, J., & Huang, H.-C. (2013). Suomi-NPP VIIRS aerosol algorithms and data products. *Journal of Geophysical Research: Atmospheres*, *118*(22), 673–689. https://doi.org/10.1002/2013JD020449

Kaufman, Y. J., Tanré, D., & Boucher, O. (2002). A satellite view of aerosols in the climate system. *Nature*, *419*(6903), 215–223. https://doi.org/10.1038/nature01091

Kaufman, Y. J., Tanré, D., Remer, L. A., Vermote, E. F., Chu, A., & Holben, B. N. (1997). Operational remote sensing of tropospheric aerosol over land from EOS moderate resolution imaging spectroradiometer. *Journal of Geophysical Research*, *102*(D14), 051–067. https://doi.org/10.1029/96JD03988

Kim, D., Gu, M., Oh, T.-H., Kim, E.-K., & Yang, H.-J. (2021). Introduction of the advanced meteorological imager of Geo-Kompsat-2a: In-orbit tests and performance validation. *Remote Sensing*, *13*(7), 1303. https://doi.org/10.3390/rs13071303

Kokhanovsky, A. A., Breon, F.-M., Cacciari, A., Carboni, E., Diner, D., Di Nicolantonio, W., et al. (2007). Aerosol remote sensing over land: A comparison of satellite retrievals using different algorithms and instruments. *Atmospheric Research*, *85*(3–4), 372–394. https://doi.org/10.1016/j.atmosres.2007.02.008

Lee, J. (2024). Comparison statistics of VIIRS version 2 Deep blue AOD against AERONET observations [Dataset]. *Zenodo*. https://doi.org/10.5281/zenodo.10729462

Lee, J., Hsu, N. C., Bettenhausen, C., Sayer, A. M., Seftor, C. J., & Jeong, M.-J. (2015). Retrieving the height of smoke and dust aerosols by synergistic use of VIIRS, OMPS, and CALIOP observations. *Journal of Geophysical Research: Atmospheres*, *120*(16), 8372–8388. https://doi.org/10.1002/2015JD023567

Lee, J., Hsu, N. C., Bettenhausen, C., Sayer, A. M., Seftor, C. J., Jeong, M.-J., et al. (2016). Evaluating the height of biomass burning smoke aerosols retrieved from synergistic use of multiple satellite sensors over Southeast Asia. *Aerosol and Air Quality Research*, *16*(11), 2831–2842. https://doi.org/10.4209/aaqr.2015.08.0506

Lee, J., Hsu, N. C., Sayer, A. M., Bettenhausen, C., & Yang, P. (2017). AERONET-based nonspherical dust optical models and effects on the VIIRS Deep Blue/SOAR over water aerosol product. *Journal of Geophysical Research: Atmospheres*, *122*, 384–401. https://doi.org/10.1002/2017JD027258

Lee, J., Hsu, N. C., Sayer, A. M., Seftor, C. J., & Kim, W. V. (2021). Aerosol layer height with enhanced spectral coverage achieved by synergy between VIIRS and OMPS-NM measurements. *IEEE Geoscience and Remote Sensing Letters*, *18*(6), 949–953. https://doi.org/10.1109/LGRS.2020.2992099

Levenberg, K. (1944). A method for the solution of certain non-linear problems in least-squares. *Quarterly of Applied Mathematics*, *2*(2), 164–168. https://doi.org/10.1090/qam/10666

Levy, R., Munchak, L., Mattoo, S., Patadia, F., Remer, L., & Holz, R. (2015). Towards a long-term global aerosol optical depth record: Applying a consistent aerosol retrieval algorithm to MODIS and VIIRS-observed reflectance. *Atmospheric Measurement Techniques*, *8*(10), 4083–4110. https://doi.org/10.5194/amt-8-4083-2015

Levy, R. C., Remer, L. A., Mattoo, S., Vermote, E. F., & Kaufman, Y. J. (2007). Second-generation operational algorithm: Retrieval of aerosol properties over land from inversion of Moderate Resolution Imaging Spectroradiometer spectral reflectance. *Journal of Geophysical Research*, *112*(D13). https://doi.org/10.1029/2006JD007811

Li, Z., Zhao, X., Kahn, R., Mishchenko, M., Remer, L., Lee, K.-H., et al. (2009). Uncertainties in satellite remote sensing of aerosols and impact on monitoring its long-term trend: A review and perspective. *Annales Geophysicae*, *27*(7), 2755–2770. https://doi.org/10.5194/angeo-27-2755-2009

Lyapustin, A., Wang, Y., Choi, M., Xiong, X., Angal, A., Wu, A., et al. (2023). Calibration of the SNPP and NOAA 20 VIIRS sensors for continuity of the MODIS climate data records. *Remote Sensing of Environment*, *295*, 113717. https://doi.org/10.1016/j.rse.2023.113717

Lyapustin, A., Wang, Y., Korkin, S., & Huang, D. (2018). MODIS Collection 6 MAIAC algorithm. *Atmospheric Measurement Techniques*, *11*(10), 5741–5765. https://doi.org/10.5194/amt-11-5741-2018

Marquardt, D. R. (1963). An algorithm for the least-squares estimation of nonlinear parameters. *SIAM Journal on Applied Mathematics*, *11*(2), 431–441. https://doi.org/10.2307/2098941

Meyer, K., Platnick, S., Holz, R., Dutcher, S., Quinn, G., & Nagle, F. (2020). Derivation of shortwave radiometric adjustments for SNPP and NOAA-20 VIIRS for the NASA MODIS-VIIRS continuity cloud products. *Remote Sensing*, *12*(24), 4096. https://doi.org/10.3390/rs12244096

NOAA National Geophysical Data Center. (2006). 2-minute Gridded Global Relief Data (ETOPO2) v2. *NOAA National Centers for Environmental Information*. https://doi.org/10.7289/V5J1012Q

Patadia, F., Levy, R. C., & Mattoo, S. (2018). Correcting for trace gas absorption when retrieving aerosol optical depth from satellite observations of reflected shortwave radiation. *Atmospheric Measurement Techniques*, *11*(6), 3205–3219. https://doi.org/10.5194/amt-11-3205-2018

Quaas, J., Stevens, B., Stier, P., & Lohmann, U. (2010). Interpreting the cloud cover - Aerosol optical depth relationship found in satellite data using a general circulation model. *Atmospheric Chemistry and Physics*, *10*(13), 6129–6135. https://doi.org/10.5194/acp-10-6129-2010

Remer, L. A., Kaufman, Y. J., Tanré, D., Mattoo, S., Chu, D. A., Martins, J. V., et al. (2005). The MODIS aerosol algorithm, products, and validation. *Journal of the Atmospheric Sciences*, *62*(4), 947–973. https://doi.org/10.1175/JAS3385.1

Salomonson, V. V., Barnes, W. L., Maymon, P. W., Montgomery, H. E., & Ostrow, H. (1989). Modis: Advanced facility instrument for studies of the Earth as a system. *IEEE Transactions on Geoscience and Remote Sensing*, *27*(2), 145–153. https://doi.org/10.1109/36.20292

Sawyer, V., Levy, R. C., Mattoo, S., Cureton, G., Shi, Y., & Remer, L. A. (2020). Continuing the MODIS Dark Target aerosol time series with VIIRS. *Remote Sensing*, *12*(2), 308. https://doi.org/10.3390/rs12020308

Sayer, A. M., Govaerts, Y., Kolmonen, P., Lipponen, A., Luffarelli, M., Mielonen, T., et al. (2020). A review and framework for the evaluation of pixel-level uncertainty estimates in satellite aerosol remote sensing. *Atmospheric Chemistry and Physics*, *13*(2), 373–404. https://doi.org/10.5194/amt-13-373-2020

Sayer, A. M., Hsu, N. C., Bettenhausen, C., Ahmad, Z., Holben, B. N., Smirnov, A., et al. (2012). SeaWiFS Ocean Aerosol Retrieval (SOAR): Algorithm, validation, and comparison with other data sets. *Journal of Geophysical Research*, *117*(D3), D03206. https://doi.org/10.1029/2011JD016599

Sayer, A. M., Hsu, N. C., Bettenhausen, C., Holz, R. E., Lee, J., Quinn, G., & Veglio, P. (2017). Cross-calibration of S-NPP VIIRS moderate-resolution reflectives solar bands against MODIS Aqua over dark water scenes. *Atmospheric Measurement Techniques*, *10*(4), 1425–1444. https://doi.org/10.5194/amt-10-1425-2017

Sayer, A. M., Hsu, N. C., Bettenhausen, C., & Jeong, M.-J. (2013). Validation and uncertainty estimates for MODIS Collection 6 "Deep Blue" aerosol data. *Journal of Geophysical Research: Atmospheres*, *118*(14), 7864–7872. https://doi.org/10.1002/jgrd.50600

Sayer, A. M., Hsu, N. C., Bettenhausen, C., Lee, J., Redemann, J., Schmid, B., & Shinozuka, Y. (2016). Extending Deep Blue aerosol retrieval coverage to cases of absorbing aerosols above clouds: Sensitivity analysis and first case studies. *Journal of Geophysical Research: Atmospheres*, *121*(9), 4830–4854. https://doi.org/10.1002/2015JD024729

Sayer, A. M., Hsu, N. C., Lee, J., Bettenhausen, C., Kim, W. V., & Smirnov, A. (2018a). Satellite Ocean aerosol retrieval (SOAR) algorithm extension to S-NPP VIIRS as part of the Deep blue aerosol project. *Journal of Geophysical Research: Atmospheres*, *123*(1), 380–400. https://doi.org/10.1002/2017JD027412

Sayer, A. M., Hsu, N. C., Lee, J., Carletta, N., Chen, S.-H., & Smirnov, A. (2017). Evaluation of NASA Deep Blue/SOAR aerosol retrieval algorithms applied to AVHRR measurements. *Journal of Geophysical Research: Atmospheres*, *122*(18), 9945–9967. https://doi.org/10.1002/2017JD026934

Sayer, A. M., Hsu, N. C., Lee, J., Kim, W. V., Burton, S., Fenn, M. A., et al. (2019). Two decades observing smoke above clouds in the south-eastern Atlantic Ocean: Deep Blue algorithm updates and validation with ORACLES field campaign data. *Atmospheric Measurement Techniques*, *12*(7), 3595–3627. https://doi.org/10.5194/amt-12-3595-2019

Sayer, A. M., Hsu, N. C., Lee, J., Kim, W. V., Dubovik, O., Dutcher, S. T., et al. (2018b). Validation of SOAR VIIRS over-water aerosol retrievals and context within the global satellite aerosol data record. *Journal of Geophysical Research: Atmospheres*, *123*(23), 496–526. https://doi.org/10.1029/2018JD029465

Sayer, A. M., Hsu, N. C., Lee, J., Kim, W. V., & Dutcher, S. T. (2019). Validation, stability, and consistency of MODIS Collection 6.1 and VIIRS Version 1 Deep Blue aerosol data over land. *Journal of Geophysical Research: Atmospheres*, *124*(8), 4658–4688. https://doi.org/10.1029/2018JD029598

Schmit, T. J., Griffith, P., Gunshor, M. M., Daniels, J. M., Goodman, S. J., & Lebair, W. J. (2017). A closer look at the ABI on the GOES-R Series. *Bulletin of the American Meteorological Society*, *98*(4), 681–698. https://doi.org/10.1175/BAMS-D-15-00230.1

Shea, Y., Fleming, G., Kopp, G., Lukashin, C., Pilewskie, P., Smith, P., et al. (2020). CLARREO pathfinder: Mission overview and current status. In *Igarss 2020—2020 IEEE international geoscience and remote sensing symposium* (pp. 3286–3289). https://doi.org/10.1109/IGARSS39084.2020

Six, D., Fily, M., Alvain, S., Henry, P., & Benoist, J.-P. (2004). Surface characterisation of the Dome Concordia area (Antarctica) as potential satellite calibration site, using Spot4/Vegetation instrument. *Remote Sensing of Environment*, *89*(1), 83–94. https://doi.org/10.1016/j.rse.2003.10.006

Spurr, R. J. D. (2006). Vlidort: A linearized pseudo-spherical vector discrete ordinate radiative transfer code for forward model and retrieval studies in multilayer multiple scattering media. *Journal of Quantitative Spectroscopy and Radiative Transfer*, *102*(2), 316–342. https://doi.org/10.1016/j.jqsrt.2006.05.005

Szopa, S., Naik, V., Adhikary, B., Artaxo, P., Berntsen, T., Collins, W. D., et al. (2021). Short-lived climate forcers. In P. Zhai, A. Pirani, S. L. Connors, C. Péan, S. Berger, N. Caud, et al. (Eds.), *Climate change 2021: The physical science basis. Contribution of working group I to the sixth assessment report of the intergovernmental panel on climate change [Masson-Delmotte* (pp. 817–922). Cambridge University Press. https://doi.org/10.1017/9781009157896.008

Tucker, C. J. (1979). Red and photographic infrared linear combinations for monitoring vegetation. *Remote Sensing of Environment*, *8*(2), 127–150. https://doi.org/10.1016/0034-4257(79)90013-0

Wolfe, R. E., Lin, G., Nishihama, M., Tewari, K. P., Tilton, J. C., & Isaacman, A. R. (2013). Suomi NPP VIIRS prelaunch and on-orbit geometric calibration and characterization. *Journal of Geophysical Research: Atmospheres*, *118*(20), 508–521. https://doi.org/10.1002/jgrd.50873

Wu, A., Xiong, X., Bhatt, R., Haney, C., Doelling, D. R., Angal, A., & Mu, Q. (2022). An assessment of SNPP and NOAA20 VIIRS RSB calibration performance in NASA SIPS reprocessed Collection-2 L1B data products. *Remote Sensing*, *14*(17), 4134. https://doi.org/10.3390/rs14174134

Zhang, H., Kondragunta, S., Laszlo, I., Liu, H., Remer, L. A., Huang, J., et al. (2016). An enhanced VIIRS aerosol optical thickness (AOT) retrieval algorithm over land using a global surface reflectance ratio database. *Journal of Geophysical Research: Atmospheres*, *121*(18), 717–738. https://doi.org/10.1002/2016JD024859